https://doi.org/10.5194/se-2021-96
Preprint. Discussion started: 10 August 2021

Solid Earth Discussions

Exhumation and erosion of the Northern Apennines, Italy: new insights from low-temperature thermochronometers

Erica D. Erlanger[1,2], Maria Giuditta Fellin[2], Sean D. Willett[2]

[1]GFZ Potsdam, Potsdam, 14473, Germany
[2]ETH Zürich, Zürich, 8092, Switzerland

Correspondence to: Erica D. Erlanger (ederlanger@gmail.com)

Abstract. Analysis of new detrital apatite fission-track (AFT) ages from modern river sands, published bedrock and detrital AFT ages, and bedrock apatite (U-Th)/He (AHe) ages from the Northern Apennines provide new insights into the spatial and temporal pattern of erosion rates through time across the orogen. The pattern of time-averaged erosion rates derived from AHe ages from the Ligurian side of the orogen illustrates slower erosion rates relative to AFT rates from the Ligurian side and relative to AHe rates from the Adriatic side. These results are corroborated by an analysis of paired AFT and AHe thermochronometer samples, which illustrate that erosion rates have generally increased through time on the Adriatic side, but have decreased through time on the Ligurian side. Using an updated kinematic model of an asymmetric orogenic wedge, with imposed erosion rates on the Ligurian side that are a factor of two slower relative to the Adriatic side, we demonstrate that cooling ages and maximum burial depths are able to replicate the pattern of measured cooling ages across the orogen and estimates of burial depth from vitrinite reflectance data. These results suggest that horizontal motion is an important component of the overall rock motion in the wedge, and that the asymmetry of the orogen has existed for at least several million years.

1 Introduction

The Apennine mountains of Italy are an active orogen characterized by contemporaneous extensional and compressional tectonics. In the Northern Apennines, these features are linked to rollback of the Adriatic slab beneath Eurasia, suggested to be active since the Oligocene (Malinverno and Ryan, 1986). The interplay between extension and compression has affected the overall tectonic evolution of the Northern Apennines and, in particular, its exhumational and topographic evolution. Low-temperature bedrock and detrital thermochronology studies have constrained the timing and rates of exhumation at the orogen-scale (e.g. Thomson et al., 2010; Malusà and Balestrieri, 2012), and at the regional scale along the extensional retrowedge (Ligurian side) of the orogen (e.g. Fellin et al., 2007) and in the frontal fold-and-thrust belt (Adriatic side) (Balestrieri et al., 1996; Carlini et al., 2013; Zattin et al., 2002). Age-elevation profiles and multiple thermochronometers have revealed spatially variable exhumation across and along strike of the orogen, and temporal variability in exhumation rates. While these findings have improved our understanding of the evolution of the Northern Apennines, a comparison between basement and detrital

https://doi.org/10.5194/se-2021-96
Preprint. Discussion started: 10 August 2021

data and between exhumation patterns across the primary drainage divide within the frame of an orogenic-scale analysis is lacking.

In this paper, we use an updated analysis method that derives long-term erosion rates from cooling ages. We derive time-averaged erosion rates for individual samples, using two different methods for constraining the initial and final geothermal gradients. We additionally calculate erosion rates through time for existing paired AFT and AHe samples, to compare with results from age-elevation transects (Thomson et al., 2010) that illustrate a change in erosion rates at 4 Ma and were interpreted to reflect an orogen-wide increase in erosion at this time. Our results suggest that the increase in exhumation is restricted to the Adriatic side of the orogen, and may have occurred later (~1–3 Ma), whereas exhumation rates decreased on the Ligurian side at ~1–5 Ma. To understand how this pattern of regional erosion rates relates to orogen-scale kinematics of the Northern Apennines, we propose an updated kinematic model that allows for crustal accretion from both frontal accretion and underplating, and variable temperature at the base of the crust. We find that the pattern of AFT, AHe, and ZHe cooling ages, and the pattern of vitrinite reflectance across the orogen are broadly consistent with the wedge kinematics for an asymmetric orogen that is dominated by frontal accretion and has slower erosion rates on the Ligurian side by a factor of two.

1.1 Structural evolution

Development of the Apenninic wedge began at ~30 Ma, due to convergence and southwest-directed subduction of the Adriatic microplate beneath Eurasia. From the late Oligocene, sediments supplied largely by the Alps were deposited as turbidite sequences into a series of northward-migrating foredeep basins (Macigno, Cervarola, and Marnoso-Arenacea Basins) (Fig. 1), which were eventually deformed and thrust during the Neogene (Ricci Lucchi, 1986). Until the Pliocene, these Tertiary foredeep basins were overridden by the Ligurian Unit (Fig. 1), a non-metamorphosed, allochthonous accretionary complex that was thrust upon the Tertiary foredeep deposits as a surficial nappe (Merla, 1952; Pini, 1999). Eocene-to-Pliocene basins formed on top of the Ligurian Unit (Epi-Ligurian Unit) (Ori and Friend, 1984; Cibin et al., 2001), which record discontinuous deposition of shallow-marine and continental sediments (Ricci Lucchi, 1986), and presently exist as denudational remnants above the Ligurian Unit. Today, the Ligurian and Epi-Ligurian Units are the highest structural units exposed in the Northern Apennines.

https://doi.org/10.5194/se-2021-96
Preprint. Discussion started: 10 August 2021

Solid Earth
Discussions
Open Access
EGU

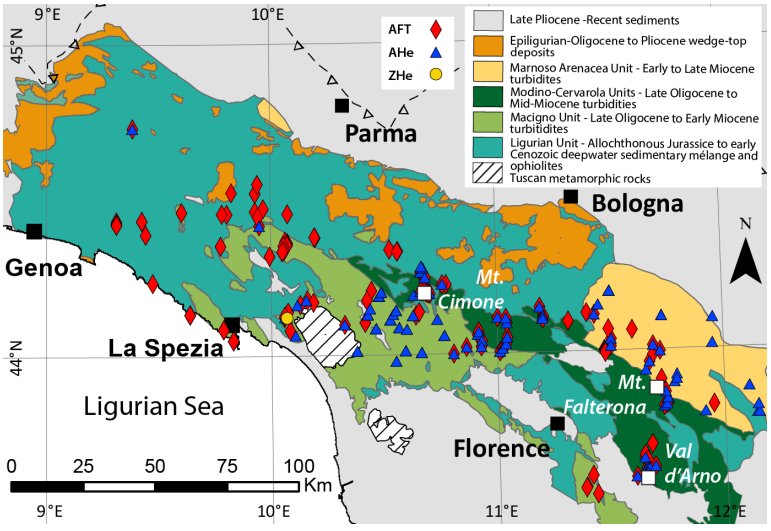

55 **Figure 1 Simplified geologic map of the Northern Apennines and locations of bedrock AFT samples (diamonds), AHe samples (triangles), and ZHe sample (circle). Dashed, sawtooth lines represent the thrust front buried beneath Po Plain sediments. The following chronostratigraphic divisions are used as minimum depositional ages for the Tertiary foredeep units: Macigno Unit (Chattian-Aquitanian) (Cita Sironi et al., 2006), Cervarola Unit (Aquitanian-Langhian) (Delfrati et al., 2002), and Marnoso Arenacea Unit (late Burdigalian-Tortonian) (Pialli et al., 2000).**

60

The onset of near-surface exhumation is constrained by the present extent and depositional ages of the Epi-Ligurian Units on the Adriatic side (Fig. 1), which are commonly not younger than the Tortonian in the NW of the study area; however, to the ESE, near Bologna, they can be as young as the Pliocene (Cibin et al., 2001). The onset of near-surface exhumation in the Northern Apennines is suggested to have begun earlier than 14 Ma, during the Tortonian (Ventura et al., 2001), although the

65 timing of the onset is debated. However, it is clear that rapid exhumation began at 8–9 Ma on the Ligurian side (Balestrieri et al., 1996), and at 4–7 Ma near the divide between the Ligurian and Adriatic sides, based on the ages and younging trend in AFT and AHe thermochronometers <10 Ma (Fig. 2) (Thomson et al., 2010).

https://doi.org/10.5194/se-2021-96
Preprint. Discussion started: 10 August 2021

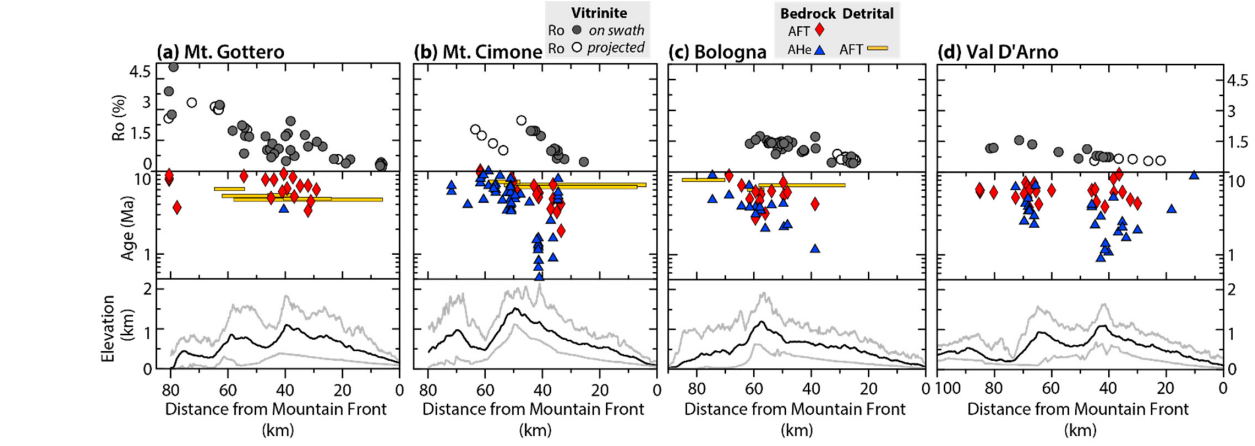

Figure 2 Vitrinite reflectance, cooling ages, and topography plotted along (a) Mt. Gottero, (b) Mt. Cimone, (c) Bologna, and (d) Val D'Arno swath profiles. Profile locations are shown in Fig. 3. (Top Row) Filled circles are vitrinite reflectance samples located within the 30 km-wide swath profile; empty circles are located outside of swath profile line and were projected onto the line. (Middle Row) Cooling ages corrected for topography for bedrock AFT (red diamonds), and AHe (blue triangles). Detrital AFT samples (yellow rectangles) were not corrected for topography. (Bottom Row) Mean elevation (thick black line), and minimum and maximum elevation (light gray lines).

The first evidence for emergent topography in the Northern Apennines is documented in the Early Pliocene, both by lacustrine deposits in an intermontane extensional basin located within the Magra River catchment (Fig. 3) (Bertoldi, 1988; Balestrieri et al., 2003), and by the exhumation of the Alpi Apuane metamorphic dome (white, hatched area in Fig. 3a) to the surface (Fellin et al., 2007). The onset of topographic relief then migrated eastward (Abbate et al., 1999; Carlini et al., 2013; Thomson et al., 2010), recorded by Pleistocene surface uplift of rocks at the drainage divide (Balestrieri et al., 2003), and the formation of Pleistocene-to-Holocene deformed fluvial terraces near the Adriatic mountain front (Picotti and Pazzaglia, 2008; Wegmann and Pazzaglia, 2009; Wilson et al., 2009).

https://doi.org/10.5194/se-2021-96
Preprint. Discussion started: 10 August 2021

Solid Earth
Discussions
Open Access
EGU

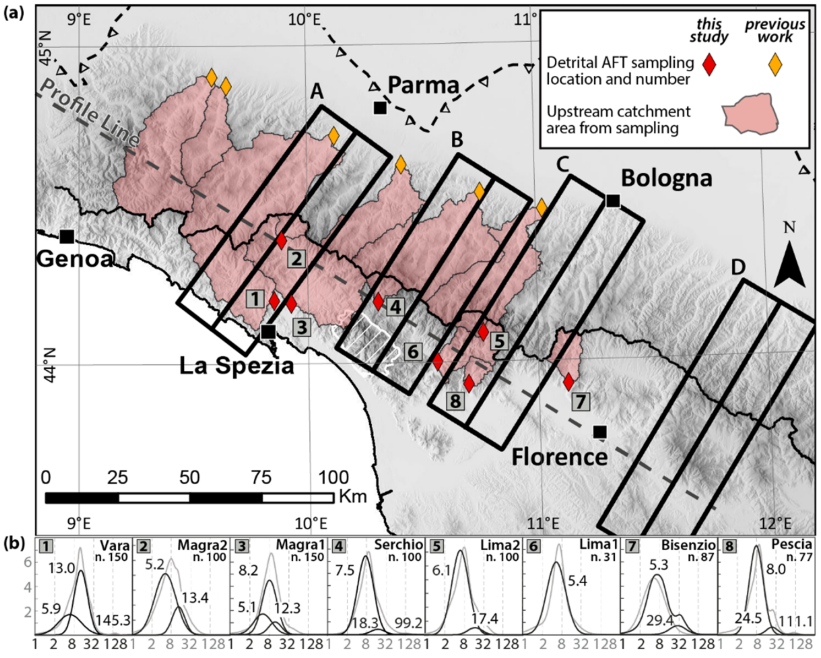

Figure 3 (a) Location map for detrital samples. Detrital AFT samples from this study are illustrated as red diamonds, and published detrital AFT samples are shown as yellow diamonds. Numbers in the gray squares correspond to the age population plots shown in (b). (b) Peak distribution curves (black curves), total PDFs (gray curves), and peak ages for all sampled Ligurian catchments.

1.2 Thermochronology data compilation

Cooling ages in the Northern Apennines are primarily limited to apatite fission track (AFT) and apatite (U-Th)/He (AHe) methods (Balestrieri et al., 1996; Ventura et al., 2001; Zattin et al., 2002; Balestrieri et al., 2003; Fellin et al., 2007; Thomson et al., 2010; Malusà and Balestrieri, 2012; Carlini et al., 2013; Balestrieri et al., 2018), as the region is dominated by sedimentary rocks (Fig. 1) that have experienced relatively low burial temperatures of less than 200–250°C (Reutter et al., 1983). Non-reset clastic rocks in the Northern Apennines are commonly exposed close to the frontal thrust zone, near the mountain front, and at high elevations (e.g. Zattin et al., 2002; Thomson et al., 2010; Carlini et al., 2013).

Maximum burial depths of rock across the Northern Apennines are constrained most commonly from vitrinite reflectance data (Fig. 2; Reutter et al., 1983; Ventura et al., 2001; Botti et al., 2004; Carlini et al., 2013), which is a proxy for burial temperatures recorded by organic particles, and is expressed as Ro (%). Higher Ro values generally reflect higher burial temperatures; Ro increases steadily from NE to SW in the Northern Apennines, with maximum Ro values near the Ligurian coastline, as shown along swath profiles in Fig. 2. This pattern of Ro values was interpreted to reflect NE-directed Miocene thrusting of the Ligurian Unit, which buried the underlying Tertiary foredeep deposits (Reutter et al., 1983).

https://doi.org/10.5194/se-2021-96
Preprint. Discussion started: 10 August 2021

2 Methods

2.1 Detrital AFT thermochronology

Bulk samples of modern sand were collected from six rivers on the Ligurian side of the Northern Apennines (Fig. 3a) and are representative of the Macigno, Alpi Apuane, and Ligurian Units (Fig. 1). As some Ligurian catchments (Magra and Serchio Rivers) contain basins with Pliocene sediments, additional samples were collected in tributaries above these basins to avoid sampling the younger, post-orogenic sediments.

Samples were processed according to the external detector method for AFT dating, using standard methods. Bulk samples were sieved and heavy minerals were separated using standard techniques, involving the use of the Wilfley table, heavy liquids, and the Frantz magnetic separator. Apatites were mounted in epoxy and were subsequently polished to expose the internal surfaces of the apatite grains. Multiple mounts per sample were produced to maximize the number of datable grains, and we aimed to date at least 100 grains per sample. However, only 37, 87, and 77 apatites were countable in samples Lima1 (6), Bisenzio (7), and Pescia (8), respectively, whereas the high number of countable apatites in samples Vara (1) and Magra1 (3) allowed us to date 150 grains in each sample.

Apatites were etched in 5.5 N HNO_3 for 20 seconds at 21 °C. AFT ages were measured and calculated using the external-detector and the zeta-calibration methods (Hurford and Green, 1983) with IUGS age standards (Durango and Fish Canyon apatites) (Hurford, 1990). The analyses were subjected to the χ^2 test (Galbraith, 1981) to assess whether the sample age distributions were over-dispersed; a probability of less than 5% denotes mixed distributions.

We determined age populations for detrital samples based on dominant age peaks identified with the Binomfit program (Brandon, 2002), which is well suited for AFT data with low spontaneous track density. In order to estimate the degree of resetting of the detrital age populations relative to the Apenninic orogenic event, we compared the detrital cooling ages with minimum depositional ages of the Tertiary foredeep units exposed in the drainage areas (Fig. 1).

2.2 Erosion rate analysis

We compiled ages from new and existing detrital AFT samples (23), bedrock AFT samples (139), AHe samples (135), and ZHe samples (26) (Tables 1–4) (Abbate et al., 1994; Balestrieri et al., 1996; Ventura et al., 2001; Zattin et al., 2002; Balestrieri et al., 2003; Fellin et al., 2007; Thomson et al., 2010; Malusà and Balestrieri, 2012; Carlini et al., 2013). As the Alpi Apuane have an erosional history different from the rest of the Northern Apennines (Balestrieri et al., 2003; Fellin et al., 2007), we removed these samples in our compilation of thermochronometric ages.

Table 1 Compilation of bedrock AHe cooling ages and sample descriptions.

https://doi.org/10.5194/se-2021-96
Preprint. Discussion started: 10 August 2021

Solid Earth
Discussions
Open Access
EGU

ID	Method	Lithology	Latitude	Longitude	Sample Elevation (km)	Mean Elevation (km)	Age (Ma)	Error (2σ)	Surface Temperature (°C)	Reference	Measured Modern Geothermal Gradient (°C/km)	Uncertainty (°C/km)	Reference
020620-3	AHe	Macigno Unit	44.122	10.068	0.756	0.383	3.66	0.22	12.19	Fellin et al. (2007)	40.0	5	della Vedova et al. (2001)
03AP34	AHe	Macigno Unit	44.066	10.107	0.285	0.340	6.89	1.22	12.40	Fellin et al. (2007)	40.0	7.5	della Vedova et al. (2001)
03AP47	AHe	PseudoMacigno Unit/Apuan autoch.*	44.128	10.259	0.890	0.870	3.60	0.22	9.75	Fellin et al. (2007)	nd	nd	della Vedova et al. (2001)
03AP51	AHe	Macigno Unit	44.014	10.380	1.060	0.688	6.85	0.41	10.66	Fellin et al. (2007)	40.0	2.5	della Vedova et al. (2001)
03AP58	AHe	PseudoMacigno Unit/Apuan autoch.*	44.003	10.308	0.305	0.665	5.86	0.35	10.77	Fellin et al. (2007)	nd	nd	della Vedova et al. (2001)
03GB04	AHe	PseudoMacigno Unit/Apuan autoch.*	43.974	10.277	0.600	0.440	5.45	0.33	11.90	Fellin et al. (2007)	nd	nd	della Vedova et al. (2001)
03GB07	AHe	Macigno Unit	44.124	10.059	0.675	0.356	5.10	0.31	12.32	Fellin et al. (2007)	40.0	7.5	della Vedova et al. (2001)
03GB09	AHe	Macigno Unit	44.162	10.115	0.335	0.546	3.51	0.21	11.37	Fellin et al. (2007)	42.5	7.5	della Vedova et al. (2001)
03GB10	AHe	Macigno Unit	44.177	10.156	0.530	0.656	6.32	0.38	10.82	Fellin et al. (2007)	42.5	7.5	della Vedova et al. (2001)
03RE19	AHe	PseudoMacigno Unit/Apuan autoch.*	44.009	10.315	0.270	0.704	4.04	0.24	10.58	Fellin et al. (2007)	nd	nd	della Vedova et al. (2001)
03RE20	AHe	Macigno Unit	44.098	10.326	1.055	0.808	4.74	0.28	10.06	Fellin et al. (2007)	40.0	5	della Vedova et al. (2001)
03AP08AB	AHe	Macigno Unit	44.190	10.632	0.880	1.295	3.36	0.20	7.63	Thomson et al. (2010)	42.5	3.5	della Vedova et al. (2001)
03AP12A	AHe	Macigno Unit	44.110	10.735	0.815	1.155	4.65	0.28	8.33	Thomson et al. (2010)	45.0	2.5	della Vedova et al. (2001)
03AP23A	AHe	Macigno Unit	44.129	10.429	0.425	0.709	9.80	0.59	10.56	Thomson et al. (2010)	40.0	2.5	della Vedova et al. (2001)
03AP23B	AHe	Macigno Unit	44.129	10.429	0.425	0.709	6.27	0.38	10.56	Thomson et al. (2010)	40.0	2.5	della Vedova et al. (2001)
03AP28A	AHe	Macigno Unit	44.111	10.529	1.035	0.899	6.60	0.40	9.60	Thomson et al. (2010)	40.0	2.5	della Vedova et al. (2001)
03AP28C	AHe	Macigno Unit	44.111	10.529	1.035	0.899	7.66	0.46	9.60	Thomson et al. (2010)	40.0	2.5	della Vedova et al. (2001)
03AP28D	AHe	Macigno Unit	44.111	10.529	1.035	0.899	6.12	0.37	9.60	Thomson et al. (2010)	40.0	2.5	della Vedova et al. (2001)
03AP29A	AHe	Macigno Unit	44.130	10.542	1.320	1.050	5.33	0.32	8.85	Thomson et al. (2010)	40.0	2.5	della Vedova et al. (2001)
03AP31A	AHe	Macigno Unit	44.142	10.553	1.815	1.131	7.40	0.44	8.44	Thomson et al. (2010)	40.0	2.5	della Vedova et al. (2001)
03AP31B	AHe	Macigno Unit	44.142	10.553	1.815	1.131	5.22	0.31	8.44	Thomson et al. (2010)	42.5	5	della Vedova et al. (2001)
03AP51C	AHe	Macigno Unit	44.014	10.380	1.060	0.688	7.92	0.48	10.66	Thomson et al. (2010)	40.0	2.5	della Vedova et al. (2001)
03AP52A	AHe	Macigno Unit	44.084	10.463	0.370	0.582	7.04	0.42	11.19	Thomson et al. (2010)	40.0	7.5	della Vedova et al. (2001)
03AP52B	AHe	Macigno Unit	44.084	10.463	0.370	0.582	7.00	0.42	11.19	Thomson et al. (2010)	40.0	7.5	della Vedova et al. (2001)
03AP52C	AHe	Macigno Unit	44.084	10.463	0.370	0.582	8.01	0.48	11.19	Thomson et al. (2010)	40.0	7.5	della Vedova et al. (2001)
03RE02	AHe	Macigno Unit	44.148	10.438	0.765	0.836	6.85	0.41	9.92	Thomson et al. (2010)	40.0	5	della Vedova et al. (2001)
03RE05A	AHe	Macigno Unit	44.188	10.480	1.495	1.138	6.73	0.40	8.41	Thomson et al. (2010)	40.0	2.5	della Vedova et al. (2001)
03RE05B	AHe	Macigno Unit	44.188	10.480	1.495	1.138	5.71	0.34	8.41	Thomson et al. (2010)	40.0	2.5	della Vedova et al. (2001)
03RE05C	AHe	Macigno Unit	44.188	10.480	1.495	0.582	8.10	0.49	11.19	Thomson et al. (2010)	42.5	7.5	della Vedova et al. (2001)
03RE05CD	AHe	Macigno Unit	44.188	10.480	1.495	1.138	9.41	0.56	8.41	Thomson et al. (2010)	40.0	2.5	della Vedova et al. (2001)
03RE05D	AHe	Macigno Unit	44.188	10.480	1.495	0.582	6.37	0.38	11.19	Thomson et al. (2010)	42.5	7.5	della Vedova et al. (2001)
03RE06A	AHe	Macigno Unit	44.201	10.488	1.640	1.194	5.93	0.36	8.13	Thomson et al. (2010)	42.5	7.5	della Vedova et al. (2001)
03RE06B	AHe	Macigno Unit	44.201	10.488	1.640	1.194	6.43	0.39	8.13	Thomson et al. (2010)	42.5	7.5	della Vedova et al. (2001)
03RE12A	AHe	Macigno Unit	44.059	10.767	0.460	0.942	5.87	0.35	9.39	Thomson et al. (2010)	45.0	7.5	della Vedova et al. (2001)
03RE12B	AHe	Macigno Unit	44.059	10.767	0.460	0.942	5.55	0.33	9.39	Thomson et al. (2010)	45.0	7.5	della Vedova et al. (2001)
03RE14A	AHe	Macigno Unit	44.005	10.665	0.840	0.635	5.28	0.32	10.92	Thomson et al. (2010)	40.0	5	della Vedova et al. (2001)
03RE14B	AHe	Macigno Unit	44.005	10.665	0.840	0.635	9.95	0.60	10.92	Thomson et al. (2010)	40.0	5	della Vedova et al. (2001)
03RE7	AHe	Macigno Unit	44.200	10.676	1.600	1.214	2.88	0.17	8.03	Thomson et al. (2010)	45.0	1.5	della Vedova et al. (2001)
03RE7R1	AHe	Macigno Unit	44.200	10.676	1.600	1.214	3.14	0.19	8.03	Thomson et al. (2010)	45.0	1.5	della Vedova et al. (2001)
03TH02	AHe	Macigno Unit	44.086	10.568	0.979	0.881	6.70	0.40	9.70	Thomson et al. (2010)	42.5	5	della Vedova et al. (2001)
03TH02B	AHe	Macigno Unit	44.086	10.568	0.979	0.881	7.51	0.45	9.70	Thomson et al. (2010)	42.5	5	della Vedova et al. (2001)
03TH12B	AHe	Macigno Unit	44.080	10.600	0.678	0.904	4.27	0.26	9.58	Thomson et al. (2010)	40.0	5	della Vedova et al. (2001)
03TH13A	AHe	Macigno Unit	44.013	10.593	0.153	0.578	8.18	0.49	11.21	Thomson et al. (2010)	40.0	5	della Vedova et al. (2001)
03TH13C	AHe	Macigno Unit	44.013	10.593	0.153	0.578	7.27	0.44	11.21	Thomson et al. (2010)	40.0	5	della Vedova et al. (2001)
03TH18A	AHe	Macigno Unit	43.980	10.552	0.047	0.449	6.74	0.40	11.85	Thomson et al. (2010)	40.0	5	della Vedova et al. (2001)
03TH23A	AHe	Macigno Unit	44.124	10.628	1.645	1.205	4.73	0.28	8.08	Thomson et al. (2010)	42.5	2.5	della Vedova et al. (2001)
03TH23BD	AHe	Macigno Unit	44.124	10.628	1.645	1.205	5.38	0.32	8.08	Thomson et al. (2010)	42.5	2.5	della Vedova et al. (2001)
03TH23C	AHe	Macigno Unit	44.124	10.628	1.645	1.205	4.55	0.27	8.08	Thomson et al. (2010)	42.5	2.5	della Vedova et al. (2001)
050320-1C	AHe	Helminthoid Flysch	44.263	10.664	1.112	1.024	1.15	0.11	8.98	Thomson et al. (2010)	42.5	3	della Vedova et al. (2001)
050320-1D	AHe	Helminthoid Flysch	44.263	10.664	1.112	1.024	1.84	0.11	8.98	Thomson et al. (2010)	42.5	3.5	della Vedova et al. (2001)
050320-2B	AHe	Helminthoid Flysch	44.276	10.674	1.239	0.965	5.28	0.32	9.27	Thomson et al. (2010)	42.5	4	della Vedova et al. (2001)
050320-2C	AHe	Helminthoid Flysch	44.276	10.674	1.239	0.965	5.42	0.33	9.27	Thomson et al. (2010)	42.5	4.5	della Vedova et al. (2001)
050320-3A	AHe	Helminthoid Flysch	44.280	10.668	1.272	0.957	9.29	0.56	9.31	Thomson et al. (2010)	42.5	5	della Vedova et al. (2001)
050320-3B	AHe	Helminthoid Flysch	44.280	10.668	1.272	0.957	6.04	0.66	9.31	Thomson et al. (2010)	42.5	5.5	della Vedova et al. (2001)
050320-3C	AHe	Helminthoid Flysch	44.280	10.668	1.272	0.957	6.61	0.40	9.31	Thomson et al. (2010)	42.5	6	della Vedova et al. (2001)

https://doi.org/10.5194/se-2021-96
Preprint. Discussion started: 10 August 2021

Solid Earth Discussions

1926	AHe	Marnoso Arenacea Unit	44.107	11.729	0.250	0.471	6.14	0.37	11.75	Thomson et al. (2010)	25.5	0.5	Pauselli et al. (2019)
1926B	AHe	Marnoso Arenacea Unit	44.107	11.729	0.250	0.471	3.16	0.19	11.75	Thomson et al. (2010)	25.5	0.5	Pauselli et al. (2019)
1926C	AHe	Marnoso Arenacea Unit	44.107	11.729	0.250	0.471	5.88	0.35	11.75	Thomson et al. (2010)	25.5	0.5	Pauselli et al. (2019)
1926D	AHe	Marnoso Arenacea Unit	44.107	11.729	0.250	0.471	2.89	0.17	11.75	Thomson et al. (2010)	25.5	0.5	Pauselli et al. (2019)
1929	AHe	Marnoso Arenacea Unit	44.037	11.504	0.700	0.702	1.65	0.10	10.59	Thomson et al. (2010)	28.5	2.5	Pauselli et al. (2019)
AP1	AHe	Marnoso Arenacea Unit	43.790	12.146	0.700	0.776	1.34	0.08	10.22	Thomson et al. (2010)	23.5	3	Pauselli et al. (2019)
AP17	AHe	Marnoso Arenacea Unit	43.876	12.110	0.600	0.605	1.94	0.12	11.07	Thomson et al. (2010)	22.5	2.5	Pauselli et al. (2019)
AP2	AHe	Marnoso Arenacea Unit	43.79	12.15	0.60	0.77	2.41	0.14	10.25	Thomson et al. (2010)	24.0	1.5	Pauselli et al. (2019)
AP3	AHe	Marnoso Arenacea Unit	43.815	12.149	0.900	0.727	3.27	0.20	10.46	Thomson et al. (2010)	23.5	1.5	Pauselli et al. (2019)
AP30	AHe	Marnoso Arenacea Unit	43.895	11.779	0.750	0.879	1.62	0.10	9.70	Thomson et al. (2010)	27.5	1.5	Pauselli et al. (2019)
AP33	AHe	Marnoso Arenacea Unit	43.919	11.792	0.650	0.801	1.29	0.08	10.09	Thomson et al. (2010)	27.0	1.5	Pauselli et al. (2019)
AP36E	AHe	Marnoso Arenacea Unit	44.097	11.955	0.370	0.271	9.54	0.77	12.74	Thomson et al. (2010)	22.5	0.5	Pauselli et al. (2019)
AP37	AHe	Marnoso Arenacea Unit	44.015	11.951	0.150	0.423	2.95	0.18	11.99	Thomson et al. (2010)	21.0	1.5	Pauselli et al. (2019)
AP38	AHe	Marnoso Arenacea Unit	43.797	11.914	1.200	0.858	1.97	0.12	9.81	Thomson et al. (2010)	26.0	6.5	Pauselli et al. (2019)
AP43R1	AHe	Marnoso Arenacea Unit	43.818	11.733	0.515	0.860	3.08	0.20	9.80	Thomson et al. (2010)	29.5	2.5	Pauselli et al. (2019)
AP43R2	AHe	Marnoso Arenacea Unit	43.818	11.733	0.515	0.860	3.35	0.20	9.80	Thomson et al. (2010)	29.5	2.5	Pauselli et al. (2019)
AP44R1	AHe	Marnoso Arenacea Unit	43.824	11.746	0.725	0.868	2.02	0.12	9.76	Thomson et al. (2010)	29.5	2.5	Pauselli et al. (2019)
AP45R1	AHe	Marnoso Arenacea Unit	43.844	11.749	0.940	0.897	3.12	0.22	9.62	Thomson et al. (2010)	29.5	2.5	Pauselli et al. (2019)
AP45R2	AHe	Marnoso Arenacea Unit	43.844	11.749	0.940	0.897	1.04	0.06	9.62	Thomson et al. (2010)	29.0	3.5	Pauselli et al. (2019)
AP47R1	AHe	Marnoso Arenacea Unit	43.864	11.739	1.365	0.906	2.33	0.14	9.57	Thomson et al. (2010)	29.0	3.5	Pauselli et al. (2019)
AP48R1	AHe	Marnoso Arenacea Unit	43.879	11.711	1.655	0.907	3.29	0.20	9.56	Thomson et al. (2010)	30.0	1.25	Pauselli et al. (2019)
AP48R2	AHe	Marnoso Arenacea Unit	43.879	11.711	1.655	0.907	3.29	0.20	9.56	Thomson et al. (2010)	30.0	1.25	Pauselli et al. (2019)
AP5	AHe	Marnoso Arenacea Unit	44.189	11.501	0.200	0.521	5.96	0.36	11.50	Thomson et al. (2010)	28.5	1.5	della Vedova et al. (2001)
AP52	AHe	Marnoso Arenacea Unit	43.905	11.791	0.565	0.836	1.92	0.12	9.92	Thomson et al. (2010)	26.5	1.5	Pauselli et al. (2019)
AP53	AHe	Marnoso Arenacea Unit	43.934	11.656	0.907	0.830	5.33	0.32	9.95	Thomson et al. (2010)	29.0	1	Pauselli et al. (2019)
AP54	AHe	Marnoso Arenacea Unit	43.961	11.670	0.690	0.811	1.93	0.12	10.05	Thomson et al. (2010)	27.5	1.5	Pauselli et al. (2019)
AP55	AHe	Marnoso Arenacea Unit	44.013	11.687	1.070	0.722	2.08	0.12	10.49	Thomson et al. (2010)	27.5	1.5	Pauselli et al. (2019)
AP57	AHe	Marnoso Arenacea Unit	43.995	11.719	0.450	0.746	1.32	0.08	10.37	Thomson et al. (2010)	27.5	0	Pauselli et al. (2019)
AP5B	AHe	Marnoso Arenacea Unit	44.189	11.501	0.200	0.521	2.15	0.13	11.50	Thomson et al. (2010)	28.5	1.5	della Vedova et al. (2001)
AP5C	AHe	Marnoso Arenacea Unit	44.189	11.501	0.200	0.521	1.01	0.06	11.50	Thomson et al. (2010)	28.5	1.5	della Vedova et al. (2001)
AP5D	AHe	Marnoso Arenacea Unit	44.189	11.501	0.200	0.521	2.72	0.16	11.50	Thomson et al. (2010)	28.5	2	della Vedova et al. (2001)
AP8	AHe	Marnoso Arenacea Unit	44.147	11.449	0.300	0.629	1.28	0.08	10.95	Thomson et al. (2010)	30.0	2.5	della Vedova et al. (2001)
AP9	AHe	Marnoso Arenacea Unit	44.115	11.431	0.400	0.674	1.37	0.08	10.73	Thomson et al. (2010)	27.5	3.75	Pauselli et al. (2019)
C1	AHe	Cervarola Unit	44.113	11.002	0.500	0.765	3.62	0.22	10.28	Thomson et al. (2010)	40.0	6	della Vedova et al. (2001)
C10	AHe	Cervarola Unit	44.143	11.191	0.605	0.766	0.79	0.05	10.27	Thomson et al. (2010)	35.0	5	della Vedova et al. (2001)
C11	AHe	Cervarola Unit	44.001	10.807	0.950	0.667	6.11	0.37	10.77	Thomson et al. (2010)	45.0	7.5	della Vedova et al. (2001)
C13	AHe	Cervarola Unit	44.021	10.864	0.700	0.747	3.87	0.23	10.37	Thomson et al. (2010)	47.5	10	della Vedova et al. (2001)
C16	AHe	Cervarola Unit	44.060	10.913	0.630	0.909	2.86	0.17	9.55	Thomson et al. (2010)	45.0	8.5	della Vedova et al. (2001)
C17	AHe	Cervarola Unit	44.068	10.919	0.625	0.921	2.80	0.17	9.49	Thomson et al. (2010)	45.0	8.5	della Vedova et al. (2001)
C2	AHe	Cervarola Unit	44.004	11.012	0.830	0.660	3.62	0.22	10.80	Thomson et al. (2010)	45.0	8.5	della Vedova et al. (2001)
C22	AHe	Cervarola Unit	44.041	10.932	0.850	0.821	3.97	0.24	10.00	Thomson et al. (2010)	45.0	8.5	della Vedova et al. (2001)
C23	AHe	Cervarola Unit	44.021	10.929	0.884	0.719	4.27	0.26	10.51	Thomson et al. (2010)	45.0	7.5	della Vedova et al. (2001)
C29	AHe	Cervarola Unit	44.731	9.386	0.320	0.775	2.84	0.17	10.23	Thomson et al. (2010)	35.0	0.5	della Vedova et al. (2001)
C3	AHe	Cervarola Unit	44.014	11.025	0.780	0.706	4.05	0.24	10.57	Thomson et al. (2010)	45.0	8	della Vedova et al. (2001)
C34	AHe	Cervarola Unit	44.417	9.949	0.510	0.855	2.73	0.16	9.83	Thomson et al. (2010)	40.0	2.5	della Vedova et al. (2001)
C37	AHe	Cervarola Unit	44.246	10.683	0.641	1.064	1.59	0.10	8.78	Thomson et al. (2010)	45.0	2.5	della Vedova et al. (2001)
C4	AHe	Cervarola Unit	44.028	11.038	0.680	0.753	1.96	0.12	10.34	Thomson et al. (2010)	43.5	8	della Vedova et al. (2001)
C40	AHe	Cervarola Unit	44.223	10.758	1.250	0.980	1.73	0.10	9.20	Thomson et al. (2010)	46.0	1	della Vedova et al. (2001)
C5	AHe	Cervarola Unit	44.049	11.044	0.610	0.798	3.64	0.22	10.11	Thomson et al. (2010)	42.5	7.5	della Vedova et al. (2001)
C52A	AHe	Cervarola Unit	44.013	11.503	0.360	0.661	3.43	0.21	10.80	Thomson et al. (2010)	28.5	4	Pauselli et al. (2019)
C6	AHe	Cervarola Unit	44.095	11.044	0.650	0.779	1.92	0.12	10.21	Thomson et al. (2010)	40.0	2.5	della Vedova et al. (2001)
C7	AHe	Cervarola Unit	44.111	11.039	0.625	0.755	2.05	0.12	10.33	Thomson et al. (2010)	40.0	2.5	della Vedova et al. (2001)
C8	AHe	Cervarola Unit	44.115	11.204	0.700	0.757	1.89	0.11	10.32	Thomson et al. (2010)	37.5	2.5	della Vedova et al. (2001)
C9	AHe	Cervarola Unit	44.106	11.204	1.000	0.738	1.62	0.10	10.41	Thomson et al. (2010)	37.5	2.5	della Vedova et al. (2001)
CIM1	AHe	Cervarola Unit (Modino)	44.194	10.699	2.165	1.174	3.35	0.20	8.23	Thomson et al. (2010)	45.0	1.5	della Vedova et al. (2001)
CIM1R1	AHe	Cervarola Unit (Modino)	44.194	10.699	2.165	1.174	3.34	0.20	8.23	Thomson et al. (2010)	45.0	1.5	della Vedova et al. (2001)
CIM2	AHe	Cervarola Unit (Modino)	44.194	10.704	2.045	1.165	2.74	0.16	8.27	Thomson et al. (2010)	45.0	1.5	della Vedova et al. (2001)
CIM3	AHe	Cervarola Unit (Modino)	44.196	10.692	1.950	1.184	2.63	0.16	8.18	Thomson et al. (2010)	45.0	1.5	della Vedova et al. (2001)
CIM3R1	AHe	Cervarola Unit (Modino)	44.196	10.692	1.950	1.184	3.55	0.21	8.18	Thomson et al. (2010)	45.0	1.5	della Vedova et al. (2001)

https://doi.org/10.5194/se-2021-96
Preprint. Discussion started: 10 August 2021

Solid Earth Discussions

CIM4	AHe	Cervarola Unit (Modino)	44.200	10.684	1.830	1.196	2.84	0.17	8.12	Thomson et al. (2010)	45.0	1.5	della Vedova et al. (2001)
CIM4R1	AHe	Cervarola Unit (Modino)	44.200	10.684	1.830	1.196	2.98	0.18	8.12	Thomson et al. (2010)	45.0	1.5	della Vedova et al. (2001)
CIM5	AHe	Cervarola Unit (Modino)	44.202	10.677	1.750	1.208	2.98	0.18	8.06	Thomson et al. (2010)	45.0	1.5	della Vedova et al. (2001)
CIM5A	AHe	Cervarola Unit (Modino)	44.202	10.677	1.750	1.208	2.69	0.16	8.06	Thomson et al. (2010)	45.0	1.5	della Vedova et al. (2001)
CIM5R1	AHe	Cervarola Unit (Modino)	44.202	10.677	1.750	1.208	2.53	0.15	8.06	Thomson et al. (2010)	45.0	1.5	della Vedova et al. (2001)
CIM6	AHe	Cervarola Unit (Modino)	44.201	10.666	1.660	1.230	2.62	0.16	7.95	Thomson et al. (2010)	45.0	1.5	della Vedova et al. (2001)
CIM6R1	AHe	Cervarola Unit (Modino)	44.201	10.666	1.660	1.230	2.68	0.16	7.95	Thomson et al. (2010)	45.0	1.5	della Vedova et al. (2001)
VALD10a	AHe	Macigno Unit	43.653	11.640	1.4	0.836	3.49	0.21	9.92	Thomson et al. (2010)	28.5	1	Pauselli et al. (2019)
VALD1a	AHe	Macigno Unit	43.594	11.603	0.497	0.471	6.94	0.42	11.75	Thomson et al. (2010)	29.0	1	Pauselli et al. (2019)
VALD2a	AHe	Macigno Unit	43.612	11.645	0.5	0.685	3.89	0.23	10.67	Thomson et al. (2010)	30.0	0.5	Pauselli et al. (2019)
VALD2R1	AHe	Macigno Unit	43.612	11.645	0.5	0.685	3.87	0.23	10.67	Thomson et al. (2010)	30.0	0.5	Pauselli et al. (2019)
VALD4a1	AHe	Macigno Unit	43.620	11.648	0.74	0.730	3.52	0.21	10.45	Thomson et al. (2010)	29.5	0.5	Pauselli et al. (2019)
VALD4a2	AHe	Macigno Unit	43.620	11.648	0.74	0.730	5.03	0.3	10.45	Thomson et al. (2010)	29.5	0.5	Pauselli et al. (2019)
VALD4R1	AHe	Macigno Unit	43.620	11.648	0.74	0.730	4.01	0.24	10.45	Thomson et al. (2010)	29.5	0.5	Pauselli et al. (2019)
VALD5a	AHe	Macigno Unit	43.621	11.656	0.85	0.747	3.96	0.24	10.36	Thomson et al. (2010)	30.0	0.5	Pauselli et al. (2019)
VALD5R1	AHe	Macigno Unit	43.621	11.656	0.85	0.747	3.92	0.23	10.36	Thomson et al. (2010)	30.0	0.5	Pauselli et al. (2019)
VALD6a	AHe	Macigno Unit	43.620	11.659	0.88	0.746	4.09	0.25	10.37	Thomson et al. (2010)	30.0	0.5	Pauselli et al. (2019)
VALD6R1	AHe	Macigno Unit	43.620	11.659	0.88	0.746	3.86	0.23	10.37	Thomson et al. (2010)	30.0	0.5	Pauselli et al. (2019)
VALD7a	AHe	Macigno Unit	43.604	11.651	1.1	0.658	3.75	0.22	10.81	Thomson et al. (2010)	31.0	0.5	Pauselli et al. (2019)
VALD8R1	AHe	Macigno Unit	43.626	11.684	1.2	0.782	4.11	0.25	10.19	Thomson et al. (2010)	30.5	0.5	Pauselli et al. (2019)
VALD8R2	AHe	Macigno Unit	43.626	11.684	1.2	0.782	3.46	0.21	10.19	Thomson et al. (2010)	30.5	0.5	Pauselli et al. (2019)

*Lithologies exposed in the Alpi Apuane metamorphic dome. These samples were excluded from the erosion rate inversions

Table 2 Compilation of bedrock AFT cooling ages and sample descriptions.

https://doi.org/10.5194/se-2021-96
Preprint. Discussion started: 10 August 2021

Solid Earth
Discussions
Open Access
EGU

ID	Method	Lithology	Latitude	Longitude	Sample Elevation (km)	Mean Elevation (km)	Age (Ma)	Error (1σ)	Surface Temperature (°C)	Reference
AR1	AFT	Pseudomacigno Apuan autochthon*	44.058	10.226	0.840	0.607	4.71	0.59	11.06	Abbate et al. (1994)
(AR2A)a	AFT	Pseudomacigno Apuan autochthon*	44.055	10.256	0.840	0.634	5.24	0.63	10.93	Abbate et al. (1994)
AR3	AFT	Pseudomacigno Apuan autochthon*	44.055	10.256	0.840	0.634	4.95	0.58	10.93	Abbate et al. (1994)
BT1	AFT	graywacke	44.085	9.787	0.475	0.104	4.58	0.78	13.58	Abbate et al. (1994)
BT2	AFT	graywacke	44.085	9.787	0.525	0.104	4.73	0.55	13.58	Abbate et al. (1994)
CB3	AFT	granite cgl	44.051	9.830	0.000	0.079	8.11	1.19	13.70	Abbate et al. (1994)
CB4	AFT	gneiss cgl	44.051	9.830	0.000	0.079	8.46	0.42	13.70	Abbate et al. (1994)
CB5	AFT	graywacke	44.051	9.830	0.000	0.079	7.13	0.67	13.70	Abbate et al. (1994)
CP1	AFT	Hercynian Basement*	44.028	10.264	0.675	0.554	3.93	0.36	11.33	Abbate et al. (1994)
CP3	AFT	Apuan autochthon*	44.017	10.264	0.650	0.554	3.64	0.71	11.33	Abbate et al. (1994)
FC3	AFT	Pseudomacigno Apuan autochthon*	44.078	10.267	1.620	0.701	5.59	0.61	10.59	Abbate et al. (1994)
FC5	AFT	Pseudomacigno Apuan autochthon*	44.078	10.267	1.620	0.701	5.95	0.59	10.59	Abbate et al. (1994)
FO1	AFT	Pseudomacigno Apuan autochthon*	44.036	10.375	0.450	0.619	1.96	0.56	11.00	Abbate et al. (1994)
FO4	AFT	Pseudomacigno Apuan autochthon*	44.033	10.375	0.425	0.610	1.91	0.31	11.05	Abbate et al. (1994)
FO5	AFT	Pseudomacigno Apuan autochthon*	44.044	10.388	0.460	0.636	1.63	0.25	10.92	Abbate et al. (1994)
G2	AFT	Hercynian Basement Apuan autochthon*	44.069	10.193	0.170	0.571	3.96	0.36	11.24	Abbate et al. (1994)
MD1 (MAD1)	AFT	Hercynian Basement*	44.040	10.192	0.787	0.502	3.86	0.77	11.59	Abbate et al. (1994)
ROM1	AFT	Marnoso Arenacea Unit	44.002	11.472	0.890	0.562	5.50	1.10	11.29	Balesterieri et al. (2018)
ROM2	AFT	Marnoso Arenacea Unit	44.001	11.472	0.760	0.560	5.00	0.70	11.30	Balesterieri et al. (2018)
ROM3	AFT	Marnoso Arenacea Unit	44.000	11.475	0.675	0.560	3.90	1.00	11.30	Balesterieri et al. (2018)
ROM4	AFT	Marnoso Arenacea Unit	43.998	11.477	0.575	0.563	4.00	1.00	11.28	Balesterieri et al. (2018)
ROM5	AFT	Marnoso Arenacea Unit	43.994	11.477	0.480	0.562	6.60	1.40	11.29	Balesterieri et al. (2018)
TCGA	AFT	Marnoso Arenacea Unit	43.993	11.476	0.360	0.560	5.00	1.60	11.30	Balesterieri et al. (2018)
CAS1	AFT	Macigno Unit	44.206	10.446	1.300	1.061	8.93	1.34	8.79	Balestrieri (2000)
CAS2	AFT	Macigno Unit	44.174	10.424	0.965	0.980	9.19	1.43	9.20	Balestrieri (2000)
CAST2	AFT	Macigno Unit	44.105	10.415	0.270	0.811	8.91	1.30	10.04	Balestrieri (2000)
CAST3	AFT	Macigno Unit	44.105	10.415	0.240	0.811	8.21	1.00	10.04	Balestrieri (2000)
GOM2	AFT	Macigno Unit	44.125	10.642	1.850	1.061	9.51	1.40	8.79	Balestrieri (2000)
GOM3	AFT	Macigno Unit	44.134	10.656	1.300	1.096	6.19	0.86	8.62	Balestrieri (2000)
BOR2	AFT	Gottero Sandstone	44.4352	9.425	0.452	0.779	7.50	1.00	10.20	Balestrieri et al. (1996)
BORI	AFT	Gottero Sandstone	44.4352	9.425	0.450	0.779	6.40	1.00	10.20	Balestrieri et al. (1996)
MG3	AFT	Gottero Sandstone	44.2345	9.472	0.000	0.193	9.70	1.10	13.13	Balestrieri et al. (1996)
MS1	AFT	Gottero Sandstone	44.1338	9.638	0.000	0.136	9.70	1.10	13.42	Balestrieri et al. (1996)
MS2	AFT	Gottero Sandstone	44.1338	9.638	0.000	0.136	7.60	0.70	13.42	Balestrieri et al. (1996)
MS4	AFT	Gottero Sandstone	44.1338	9.638	0.000	0.136	8.00	1.20	13.42	Balestrieri et al. (1996)
MS5	AFT	Gottero Sandstone	44.1338	9.638	0.000	0.136	8.70	1.20	13.42	Balestrieri et al. (1996)
RAM1	AFT	Gottero Sandstone	44.434	9.311	1.318	0.632	8.60	1.10	10.94	Balestrieri et al. (1996)
RAM3	AFT	Gottero Sandstone	44.4268	9.312	1.075	0.606	6.50	1.10	11.07	Balestrieri et al. (1996)
RAM4	AFT	Gottero Sandstone	44.4268	9.312	1.075	0.606	7.50	1.00	11.07	Balestrieri et al. (1996)
RAM5	AFT	Gottero Sandstone	44.4221	9.311	0.950	0.587	7.30	0.80	11.17	Balestrieri et al. (1996)
RAM6	AFT	Gottero Sandstone	44.4221	9.311	0.948	0.587	6.50	0.70	11.17	Balestrieri et al. (1996)
ZAT2	AFT	Gottero Sandstone	44.3908	9.442	1.349	0.637	9.50	1.30	10.92	Balestrieri et al. (1996)
CH1	AFT	Macigno Unit	43.601	11.411	0.303	0.337	5.60	0.90	12.42	Bonini et al. (2013)
CH2	AFT	Macigno Unit	43.541	11.430	0.504	0.379	6.10	1.00	12.20	Bonini et al. (2013)
CH3	AFT	Macigno Unit	43.565	11.382	0.722	0.373	6.90	0.90	12.24	Bonini et al. (2013)
CH4	AFT	Macigno Unit	43.562	11.380	0.857	0.376	7.40	1.00	12.22	Bonini et al. (2013)
PR 11	AFT	Subligurian	44.463	9.930	0.880	0.808	8.70	1.10	10.06	Carlini et al. (2013)
PR 12	AFT	Tuscan Nappe	44.353	9.776	0.668	0.700	8.70	1.20	10.60	Carlini et al. (2013)
PR 15	AFT	Ligurian	44.472	9.966	1.085	0.837	7.30	1.90	9.92	Carlini et al. (2013)
PR 17	AFT	Ligurian	44.379	10.196	0.860	1.001	4.10	0.50	9.10	Carlini et al. (2013)
PR 18	AFT	Subligurian	44.380	10.194	0.780	1.001	4.60	0.80	9.10	Carlini et al. (2013)
PR 20	AFT	Tusc.	44.338	10.528	0.500	0.881	2.30	0.30	9.69	Carlini et al. (2013)
PR 22	AFT	Subligurian	44.331	10.564	1.082	0.851	2.50	0.50	9.84	Carlini et al. (2013)
PR 23.1	AFT	Ligurian	44.329	10.562	1.111	0.861	4.70	0.90	9.79	Carlini et al. (2013)
PR 25.1	AFT	Tuscan Nappe	44.320	9.995	0.248	0.639	7.00	0.90	10.91	Carlini et al. (2013)
PR 26	AFT	Tuscan Nappe	44.463	9.602	1.135	0.883	5.40	0.90	9.68	Carlini et al. (2013)
PR 27	AFT	Epiligurian	44.525	9.824	0.618	0.726	4.70	1.00	10.47	Carlini et al. (2013)
PR 28.1	AFT	Ligurian	44.522	9.931	0.710	0.776	3.20	0.50	10.22	Carlini et al. (2013)
PR 28.2	AFT	Ligurian	44.522	9.931	0.702	0.776	4.10	0.60	10.22	Carlini et al. (2013)
PR 3	AFT	Tuscan Nappe	44.446	9.943	0.600	0.817	6.20	1.00	10.01	Carlini et al. (2013)

https://doi.org/10.5194/se-2021-96
Preprint. Discussion started: 10 August 2021

PR 5	AFT	Ligurian	44.456	9.804	0.718	0.777	7.80	0.80	10.21	Carlini et al. (2013)
PR 6.1	AFT	Subligurian	44.456	9.783	0.600	0.789	4.30	0.90	10.15	Carlini et al. (2013)
PR 7	AFT	Subligurian	44.550	9.940	0.301	0.748	4.90	1.00	10.36	Carlini et al. (2013)
03GB07	AFT	Macigno Unit	44.124	10.059	0.675	0.356	7.90	0.90	12.32	Felin et al. (2007)
03RE20	AFT	Macigno Unit	44.098	10.326	1.055	0.760	7.50	1.00	10.30	Felin et al. (2007)
MSV 2	AFT	Pseudomacigno Apuan*	44.106	10.288	0.654	0.752	5.70	0.75	10.34	Felin et al. (2007)
S 1	AFT	Macigno Unit	44.178	10.160	0.546	0.662	6.50	0.95	10.79	Felin et al. (2007)
S 3	AFT	Macigno Unit	44.139	10.073	0.494	0.374	6.60	0.85	12.23	Felin et al. (2007)
S 4	AFT	Macigno Unit	44.128	10.059	0.636	0.330	5.10	0.85	12.45	Felin et al. (2007)
SC 2	AFT	Macigno Unit	44.081	10.083	0.204	0.342	6.40	1.10	12.39	Felin et al. (2007)
SM 3	AFT	Macigno Unit	44.164	10.129	0.250	0.558	8.80	1.40	11.31	Felin et al. (2007)
SU 1	AFT	Macigno Unit	44.170	10.188	0.773	0.724	6.50	1.05	10.48	Felin et al. (2007)
050320-1a	AFT	Helminthoid Flysch	44.263	10.664	1.112	0.976	7.30	2.30	9.22	Thomson et al. (2010)
050320-1b	AFT	Helminthoid Flysch	44.263	10.664	1.112	0.976	5.00	1.30	9.22	Thomson et al. (2010)
CIM1	AFT	Cervarola Unit (Modino)	44.194	10.699	2.165	1.121	7.53	NA	8.50	Thomson et al. (2010)
CIM2	AFT	Cervarola Unit (Modino)	44.194	10.704	2.045	1.116	7.84	NA	8.52	Thomson et al. (2010)
CIM3	AFT	Cervarola Unit (Modino)	44.196	10.692	1.950	1.124	7.44	NA	8.48	Thomson et al. (2010)
CIM4	AFT	Cervarola Unit (Modino)	44.200	10.684	1.830	1.128	6.68	NA	8.46	Thomson et al. (2010)
CIM5	AFT	Cervarola Unit (Modino)	44.202	10.677	1.750	1.134	7.22	NA	8.43	Thomson et al. (2010)
CIM6	AFT	Cervarola Unit (Modino)	44.201	10.666	1.660	1.149	6.60	NA	8.35	Thomson et al. (2010)
SILL1	AFT	Macigno Unit	44.368	10.064	1.861	0.860	8.70	NA	9.80	Thomson et al. (2010)
SILL10	AFT	Macigno Unit	44.334	10.050	0.730	0.754	7.10	NA	10.33	Thomson et al. (2010)
SILL2	AFT	Macigno Unit	44.361	10.074	1.790	0.863	9.60	NA	9.78	Thomson et al. (2010)
SILL3	AFT	Macigno Unit	44.357	10.073	1.600	0.853	6.60	NA	9.84	Thomson et al. (2010)
SILL4	AFT	Macigno Unit	44.455	10.076	1.530	0.951	5.80	NA	9.34	Thomson et al. (2010)
SILL5	AFT	Macigno Unit	44.354	10.071	1.420	0.843	6.80	NA	9.89	Thomson et al. (2010)
SILL6	AFT	Macigno Unit	44.353	10.057	1.260	0.815	6.80	NA	10.03	Thomson et al. (2010)
SILL7	AFT	Macigno Unit	44.338	10.058	1.130	0.781	6.10	NA	10.19	Thomson et al. (2010)
SILL9	AFT	Macigno Unit	44.334	10.050	0.780	0.755	5.30	NA	10.32	Thomson et al. (2010)
VALD1	AFT	Macigno Unit	43.594	11.603	0.497	0.484	4.97	NA	11.68	Thomson et al. (2010)
VALD10	AFT	Macigno Unit	43.653	11.640	1.400	0.836	7.33	NA	9.92	Thomson et al. (2010)
VALD11	AFT	Macigno Unit	43.663	11.641	1.450	0.644	6.12	NA	10.88	Thomson et al. (2010)
VALD12	AFT	Macigno Unit	43.696	11.673	0.960	0.717	6.63	NA	10.51	Thomson et al. (2010)
VALD2	AFT	Macigno Unit	43.612	11.645	0.500	0.550	7.35	NA	11.35	Thomson et al. (2010)
VALD3	AFT	Macigno Unit	43.614	11.656	0.580	0.559	6.73	NA	11.31	Thomson et al. (2010)
VALD4	AFT	Macigno Unit	43.620	11.648	0.740	0.567	5.35	NA	11.27	Thomson et al. (2010)
VALD5	AFT	Macigno Unit	43.621	11.656	0.850	0.572	4.43	NA	11.24	Thomson et al. (2010)
VALD6	AFT	Macigno Unit	43.620	11.659	0.880	0.571	6.83	NA	11.25	Thomson et al. (2010)
VALD7	AFT	Macigno Unit	43.604	11.651	1.100	0.536	6.88	NA	11.42	Thomson et al. (2010)
VALD8	AFT	Macigno Unit	43.626	11.684	1.200	0.585	8.84	NA	11.18	Thomson et al. (2010)
VALD9	AFT	Macigno Unit	43.646	11.652	1.200	0.619	8.58	NA	11.00	Thomson et al. (2010)
C1	AFT	Cervarola Unit	44.113	11.002	0.500	0.789	6.70	0.08	10.15	Ventura et al. (2001)
C10	AFT	Cervarola Unit	44.143	11.191	0.605	0.683	3.90	0.80	10.68	Ventura et al. (2001)
C11	AFT	Macigno Unit	44.001	10.807	0.950	0.644	9.80	1.20	10.88	Ventura et al. (2001)
C13	AFT	Modino	44.021	10.864	0.700	0.731	6.80	0.90	10.45	Ventura et al. (2001)
C16	AFT	Cervarola Unit	44.060	10.913	0.630	0.807	2.70	0.80	10.07	Ventura et al. (2001)
C17	AFT	Cervarola Unit	44.068	10.919	0.625	0.818	4.90	1.20	10.01	Ventura et al. (2001)
C2	AFT	Cervarola Unit	44.004	11.012	0.830	0.548	6.50	0.80	11.36	Ventura et al. (2001)
C22	AFT	Cervarola Unit	44.041	10.932	0.850	0.747	3.00	1.10	10.36	Ventura et al. (2001)
C23	AFT	Cervarola Unit	44.021	10.929	0.884	0.689	5.20	1.00	10.65	Ventura et al. (2001)
C29	AFT	Cervarola Unit	44.731	9.386	0.320	0.804	4.70	NA	10.08	Ventura et al. (2001)
C3	AFT	Cervarola Unit	44.014	11.025	0.780	0.580	5.00	0.05	11.20	Ventura et al. (2001)
C34	AFT	Cervarola Unit	44.417	9.949	0.510	0.820	8.60	NA	10.00	Ventura et al. (2001)
C37	AFT	Cervarola Unit	44.246	10.683	0.641	1.016	2.60	0.50	9.02	Ventura et al. (2001)
C38	AFT	Cervarola Unit	44.223	10.777	0.980	0.950	3.10	1.10	9.35	Ventura et al. (2001)
C4	AFT	Cervarola Unit	44.028	11.038	0.680	0.620	3.30	0.50	11.00	Ventura et al. (2001)
C40	AFT	Cervarola Unit	44.223	10.758	1.250	0.977	4.10	0.50	9.22	Ventura et al. (2001)
C5	AFT	Cervarola Unit	44.049	11.044	0.610	0.679	5.70	0.60	10.71	Ventura et al. (2001)
C52	AFT	Cervarola Unit	44.013	11.503	0.360	0.594	5.90	1.10	11.13	Ventura et al. (2001)
C6	AFT	Cervarola Unit	44.095	11.044	0.650	0.735	5.00	0.60	10.42	Ventura et al. (2001)
C7	AFT	Cervarola Unit	44.111	11.039	0.625	0.738	5.40	0.70	10.41	Ventura et al. (2001)
C8	AFT	Cervarola Unit	44.115	11.207	0.700	0.680	6.20	0.60	10.70	Ventura et al. (2001)
C9	AFT	Cervarola Unit	44.106	11.204	1.000	0.673	7.40	0.70	10.73	Ventura et al. (2001)
1927	AFT	Marnoso Arenacea Unit	44.064	11.597	0.350	0.667	8.50	NA	10.77	Zattin et al. (2002)

https://doi.org/10.5194/se-2021-96
Preprint. Discussion started: 10 August 2021

1929	AFT	Marnoso Arenacea Unit	44.037	11.504	0.700	0.619	6.40	0.70	11.00	Zattin et al. (2002)
1930	AFT	Marnoso Arenacea Unit	44.069	11.492	1.150	0.630	4.70	NA	10.95	Zattin et al. (2002)
AP 10	AFT	Marnoso Arenacea Unit	44.121	11.396	0.500	0.685	3.90	0.70	10.67	Zattin et al. (2002)
Ap 15	AFT	Marnoso Arenacea Unit	43.819	11.952	0.700	0.805	9.20	1.40	10.07	Zattin et al. (2002)
AP 34	AFT	Macigno Unit	44.097	11.315	0.600	0.653	5.90	0.80	10.83	Zattin et al. (2002)
AP 43	AFT	Marnoso Arenacea	43.818	11.733	0.515	0.805	5.30	0.80	10.08	Zattin et al. (2002)
AP 45	AFT	Marnoso Arenacea	43.828	11.749	0.940	0.809	4.70	0.70	10.06	Zattin et al. (2002)
AP 52	AFT	Marnoso Arenacea Unit	43.905	11.723	0.565	0.799	5.10	0.80	10.11	Zattin et al. (2002)
AP 53	AFT	Marnoso Arenacea Unit	43.934	11.656	0.907	0.814	8.60	1.10	10.03	Zattin et al. (2002)
AP 54	AFT	Marnoso Arenacea	43.961	11.670	0.690	0.747	5.60	0.70	10.36	Zattin et al. (2002)
AP 55	AFT	Marnoso Arenacea Unit	44.013	11.687	1.070	0.672	7.90	0.80	10.74	Zattin et al. (2002)
AP 56	AFT	Marnoso Arenacea Unit	43.983	11.686	0.500	0.723	4.10	0.70	10.49	Zattin et al. (2002)
AP 57	AFT	Marnoso Arenacea Unit	43.995	11.719	0.450	0.688	3.60	0.50	10.66	Zattin et al. (2002)
AP 9	AFT	Marnoso Arenacea Unit	44.115	11.431	0.400	0.673	3.90	0.70	10.73	Zattin et al. (2002)
AP44	AFT	Marnoso Arenacea Unit	43.824	11.746	0.725	0.807	6.00	0.90	10.07	Zattin et al. (2002)
AP47	AFT	Marnoso Arenacea	43.864	11.739	1.365	0.816	5.20	0.90	10.02	Zattin et al. (2002)

*Lithologies exposed in the Alpi Apuane metamorphic dome. These samples were excluded from the erosion rate inversions

Table 3 Compilation of detrital AFT cooling ages and sample descriptions.

ID	Method	Lithology	Latitude	Longitude	Sample Elevation (km)	Age (Ma)	Error (2σ)	Error (1σ)	Reference
Enza	AFT	Ligurian/EpiLigurian/Macigno	44.620	10.413	0.163	4.70	1.00	0.50	Malusa and Balestrieri (2012)
Nure	AFT	Ligurian	44.872	9.647	0.208	4.10	1.60	0.80	Malusa and Balestrieri (2012)
Panaro	AFT	Ligurian/EpiLigurian/Macigno	44.477	11.027	0.099	6.90	2.20	1.10	Malusa and Balestrieri (2012)
Secchia	AFT	Ligurian/EpiLigurian/Macigno	44.532	10.758	0.119	6.50	1.80	0.90	Malusa and Balestrieri (2012)
Taro	AFT	Ligurian/ EpiLigurian	44.713	10.120	0.117	4.60	1.60	0.80	Malusa and Balestrieri (2012)
Trebbia	AFT	Ligurian	44.901	9.584	0.140	4.00	1.40	0.70	Malusa and Balestrieri (2012)
Bisenzio	AFT	Cervarola and Modino Units	43.928	11.126	0.102	5.30	0.95	0.50	*this study*
Lima1	AFT	Cervarola/Modino/Macigno Units	44.000	10.560	0.097	5.40	1.15	0.60	*this study*
Lima2	AFT	Cervarola/Modino/Macigno Units	44.091	10.760	0.544	6.10	0.85	0.45	*this study*
Magra1	AFT	Ligurian and Macigno Units	44.188	9.925	0.036	5.10	3.10	1.50	*this study*
Magra2	AFT	Macigno and Ligurian Units	44.387	9.887	0.251	5.20	1.00	0.50	*this study*
Pescia	AFT	Macigno Unit	43.929	10.693	0.105	8.00	1.00	0.50	*this study*
Serchio	AFT	Macigno Unit	44.192	10.306	0.525	7.50	1.05	0.50	*this study*
Vara	AFT	Ligurian and Macigno Units	44.198	9.851	0.032	5.90	2.50	1.25	*this study*

Table 4 Compilation of bedrock ZHe cooling ages and sample descriptions.

https://doi.org/10.5194/se-2021-96
Preprint. Discussion started: 10 August 2021

Solid Earth Discussions

ID	Method	Lithology	Latitude	Longitude	Sample Elevation (km)	Age (Ma)	Error (2σ)	Mean Elevation (km)	Surface Temperature (°C)	Reference
CP3(4)	Zhe	Hercynian Basement Apuan autoch.*	44.017	10.264	0.650	4.98	0.40	0.405	12.075	Abbate et al. (1994)
G3(4) (G3A)a	Zhe	Hercynian Basement Apuan autoch.*	44.067	10.199	0.170	5.7	0.46	0.451	11.843	Abbate et al. (1994)
020620-1	ZHe	PseudoMacigno Unit/Apuan autoch.*	44.096	10.325	0.958	3.61	0.29	0.708	10.560	Fellin et al. (2007)
020620-3	ZHe	Macigno Unit	44.122	10.068	0.756	9.35	0.75	0.395	12.125	Fellin et al. (2007)
020620-3 rep	ZHe	Macigno Unit	44.122	10.068	0.756	9.27	0.74	0.395	12.125	Fellin et al. (2007)
03AP38	ZHe	Met. Mesozoic succ. Massa Unit*	44.069	10.139	0.925	5.94	0.47	0.392	12.140	Fellin et al. (2007)
03AP41	ZHe	Hercynian Basement Massa Unit*	44.050	10.161	0.080	6.44	0.52	0.387	12.164	Fellin et al. (2007)
03AP42	ZHe	Hercynian Basement Apuan autoch.*	44.069	10.175	0.125	7.19	0.58	0.430	11.949	Fellin et al. (2007)
03AP43	ZHe	Hercynian Basement Massa Unit*	44.048	10.179	0.505	5.11	0.41	0.399	12.104	Fellin et al. (2007)
03AP45	ZHe	Hercynian Basement Massa Unit*	44.032	10.194	0.810	5.93	0.47	0.386	12.172	Fellin et al. (2007)
03AP47	ZHe	PseudoMacigno Unit/Apuan autoch.*	44.128	10.259	0.890	4.62	0.37	0.693	10.634	Fellin et al. (2007)
03AP58	ZHe	PseudoMacigno Unit/Apuan autoch.*	44.003	10.308	0.305	4.33	0.35	0.410	12.050	Fellin et al. (2007)
03GB02	ZHe	Hercynian Basement Apuan autoch.*	43.995	10.248	0.080	5.41	0.43	0.356	12.318	Fellin et al. (2007)
03GB04	ZHe	PseudoMacigno Unit/Apuan autoch.*	43.974	10.277	0.600	6.93	0.55	0.333	12.434	Fellin et al. (2007)
03GB06	ZHe	PseudoMacigno Unit/Apuan autoch.*	43.966	10.330	0.440	5.98	0.48	0.348	12.358	Fellin et al. (2007)
03GB12	ZHe	PseudoMacigno Unit/Apuan autoch.*	44.013	10.303	0.670	5.09	0.41	0.428	11.958	Fellin et al. (2007)
03RE17	ZHe	Hercynian Basement Apuan autoch.*	44.036	10.253	0.799	5.29	0.42	0.437	11.917	Fellin et al. (2007)
03RE21	ZHe	PseudoMacigno Unit/Apuan autoch.*	44.075	10.327	0.810	6.40	0.51	0.645	10.875	Fellin et al. (2007)
03RE22	ZHe	PseudoMacigno Unit/Apuan autoch.*	44.066	10.324	0.510	4.77	0.38	0.611	11.043	Fellin et al. (2007)
03RE24	ZHe	PseudoMacigno Unit/Apuan autoch.*	44.159	10.200	0.915	5.58	0.45	0.666	10.771	Fellin et al. (2007)
03RE25A	ZHe	Hercynian Basement Apuan autoch.*	44.133	10.186	1.500	5.42	0.43	0.582	11.190	Fellin et al. (2007)
03RE27	ZHe	Hercynian Basment Massa Unit*	44.071	10.155	0.500	5.54	0.44	0.412	12.040	Fellin et al. (2007)
APUANE-1z1	ZHe	Hercynian Basement Apuan autoch.*	44.024	10.243	0.845	4.81	0.38	0.404	12.081	Fellin et al. (2007)
APUANE-1z2	ZHe	Hercynian Basement Apuan autoch.*	44.024	10.243	0.845	4.58	0.37	0.404	12.081	Fellin et al. (2007)
FIO4z2	ZHe	PseudoMacigno Unit/Apuan autoch.*	44.077	10.265	1.450	4.92	0.39	0.560	11.301	Fellin et al. (2007)
FO4A	ZHe	PseudoMacigno Unit/Apuan autoch.*	44.033	10.375	0.450	5.86	0.47	0.576	11.219	Fellin et al. (2007)

*Lithologies exposed in the Alpi Apuane metamorphic dome. These samples were excluded from the erosion rate inversions

We converted ages to erosion rates using a half-space cooling model and a closure temperature concept (Willett and Brandon, 2013). This model has the advantage of including an accurate representation of the transience associated with whole lithosphere geotherms. Reset ages were converted to erosion rates using the closure temperature concept (Dodson, 1979), with closure temperatures specific to each thermochronometer, although this is a simplification of diffusional daughter product loss that neglects effects associated with complex cooling histories. For monotonic cooling histories, the measured age of the sample is represented by the time needed for a rock to move from the closure depth to the surface (e.g. Reiners and Brandon, 2006).

The conversion to erosion rates was performed using the AGE2EDOT program, (Willett and Brandon, 2013), which estimates an erosion rate through solution of the 1-D thermal advection, diffusion problem for a lithospheric column subjected to a constant rate of erosion. Thermochronometric data required for the calculations include the measured ages and kinetic parameters from which a closure temperature is calculated. In addition, the thermal initial and boundary conditions, as well as thermal parameters, must be specified for each sample site.

For the kinetic parameters for AHe, we assumed grain sizes of 45 μm, given that sizes of dated grains are not reported by previous studies, and that a grain size of 60 μm is larger than the mean size of detrital apatites that are typically dated in the Northern Apennines. Thermal parameters (see definitions in Table 5) include an estimate for the age of onset of erosion (t_1);

https://doi.org/10.5194/se-2021-96
Preprint. Discussion started: 10 August 2021

the sample elevation, given as an elevation above a regional mean (h); surface temperature (T_s); and either an initial geothermal gradient (G_0) or the final geothermal gradient (G_f). Only one estimate of the geothermal gradient is needed, but we took several approaches, as will be discussed below. To calculate T_s, we adjusted a base temperature value for the elevation of each sample, given a lapse rate of 5°C /km. For the base temperature, we used a modern surface temperature of 13.8°C, which represents the calculated yearly average for an elevation of 53 m at Bologna from 1813–2004 (NOAA Global Temperature Summary of the Year dataset).

Table 5 Definitions of thermal parameters used in the erosion rate analysis.

Parameter	Description
G_{0_25}	Initial geothermal gradient of 25˚C/km (AGE2EDOT input)
G_{f_25}	Inferred final geothermal gradient (AGE2EDOT (output)
$G_{0\_heatflow}$	Inferred initial geothermal gradient (AGE2EDOT output)
$G_{f\_heatflow}$	Final geothermal gradient calculated from modern heat flow measurements (AGE2EDOT input)
h	Sample elevation above the regional mean elevation
tau	Thermochronometer cooling age
t_{trans}	Transition time between AFT and AHe cooling intervals
T_0	Temperature at transition time t_{trans}
T_s	Modern surface temperature

The geothermal gradient is the most important parameter incorporated into the erosion rate analysis and is also the largest source of uncertainty. It can be specified either as a final geothermal gradient (G_f), which is the present geothermal gradient at the surface, or as an initial geothermal gradient (G_0) that is assumed to be constant with depth at the onset of exhumation (Willett and Brandon, 2013). We calculated and compared erosion rates derived using two approaches. In the first method, we imposed a spatially constant G_0 of 25°C/km (G_{0_25}) (Balestrieri et al., 2003; Ventura et al., 2001; Zattin et al., 2002). In the second method, we assumed that the present-day geothermal gradient (G_f) matches the geothermal gradient calculated from geothermal heat flow measurements. We converted the heat flow measurements to a G_f ($G_{f\_heatflow}$) using a spatially constant thermal conductivity value for sandstone (2 W/mK). Heat flow values were extracted from contour maps that interpolate geothermal well data (Pauselli et al., 2019; della Vedova et al., 2001). The della Vedova et al. (2001) flow map covers the entire study area, whereas the Pauselli et al. (2019) map covers the area south of 44.5°N and includes only the Bisenzio River (Fig. 3) within the study area. Because the heat flow map of della Vedova et al. (2001) is based on fewer geothermal well measurements relative to the Pauselli et al. (2019) map, we consider the della Vedova et al. (2001) interpolation to have higher uncertainties. Thus, where the Pauselli et al. (2019) map was available, a heat flow value was selected from this map. Otherwise, a heat flow value was selected from the della Vedova et al. (2001) map.

The modelling procedure described above was applied to all ages, assuming that erosion initiated over the entire region at 10 Ma. The resulting erosion rate applies from the onset of exhumation at 10 Ma to the present and reflects the time-averaged

https://doi.org/10.5194/se-2021-96
Preprint. Discussion started: 10 August 2021

erosion rate constrained to pass through the closure temperature at the age and with a cooling rate commensurate with the average erosion rate. Thus, this method is limited to a single, average erosion rate. However, changes in exhumation rates through time in the Northern Apennines are supported by several lines of evidence, particularly by age-elevation transects (AETs). In fact, AETs from the existing literature illustrate differences along the age-elevation slope for a single thermochronometer (as in Balestrieri et al., 1999) or among age-elevation slopes for multiple thermochronometers (as in Thomson et al., 2010).

It is possible to use AGE2EDOT in an incremental manner, allowing us to use paired thermochronometers analyzed from a single sample. In this case, the temporal range of exhumation is bracketed by the AFT and AHe ages, with independent erosion rates determined from each age, thus resolving two time intervals (Willett et al., 2020). In principle, this violates the assumption of a constant rate of cooling implicit to use of the closure age concept, but provided that the transition between erosion rate intervals is not close to either age, the error will be small. We analyzed 30 available paired ages to detect temporal changes in erosion rate. For the paired ages analysis, the exhumation path is divided into two segments: the first segment extends from the onset of exhumation to a specified transition time (t_{trans}) after cooling through the AFT system, and the second segment extends from this transition time to the present, thus passing through the AHe age in this second interval (Fig. 4). We derive an erosion rate for each of these time-segments by analyzing each segment with AGE2EDOT, linking the two solutions at t_{trans}. The solutions are matched by noting the depth and temperature of the sample at t_{trans}, based on the erosion rate in the second interval, and using this and the geothermal gradient at t_{trans} as the boundary conditions for calculations of the first interval (Fig. 4).

The difference in age between some of our paired ages is less than 1 Ma, but larger than 0.5 Ma, so we set the transition at 0.5 Ma before the AHe closure for all samples (i.e. the AHe cooling age plus 0.5 Ma), in order to allow the onset of advection to precede the AHe closure. Calculation of the erosion rate over the second interval requires the modern surface temperature (T_S); the sample elevation above the regional mean (h); the AHe cooling age (tau); the final geothermal gradient as derived from heat-flow measurements ($G_{f\_heatflow}$); and the length of the time interval (t_{trans}), calculated as the AHe age plus 0.5 Ma. The erosion rate is then solved from these data and the kinetic parameters.

To calculate the erosion rate for the first interval, we require in addition, the temperature at t_{trans} (T_0) (Fig. 4); the sample elevation above the regional mean (h); the sample AFT age (tau), and the time of onset of erosion, taken as 10 Ma. To match solutions at t_{trans}, we simply reduce the age by t_{trans}, and reduce the elevation by the amount of exhumation that occurred during the second interval. We take the initial geothermal gradient obtained from the model for the second interval as the final condition for the first interval.

https://doi.org/10.5194/se-2021-96
Preprint. Discussion started: 10 August 2021

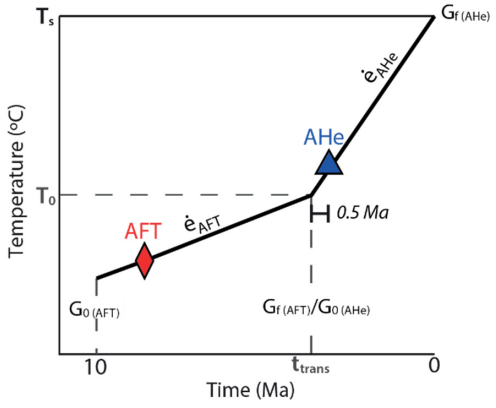

225 **Figure 4 Schematic of paired ages erosion rates analysis, illustrating the theoretical temperature path through time for a sample with paired AFT and AHe cooling ages, given the thermal parameters described in the text. ė represents the erosion rate for each interval.**

2.3 Kinematic model

230 The kinematic model presented here approximates the Northern Apennines as a doubly tapering, asymmetric wedge, given the geometric parameters illustrated in Fig. 5. The Adriatic and Ligurian sides of the orogen are defined as the accreting prowedge and non-accreting retrowedge of the orogen, respectively (e.g. Willett et al., 2001). The geometry of the wedge is defined by surface and basal angles for the prowedge (α_P and β_P) and retrowedge (α_R and β_R). The lengths of the prowedge (L_P) and retrowedge (L_R) are 60 km and 40 km, respectively, based on average widths measured from an SRTM 90 Digital Elevation
235 Model (DEM). The maximum crustal thickness is 56 km (Spada et al., 2013), the maximum elevation is 2 km, and the thickness of the accreted crust is 20 km, partitioned between frontal accretion (h_0 = 10 km) and prowedge basal accretion (h_1 = 10 km). We assume no retrowedge accretion (h_2 = 0). Closure depths are set for ZHe (7.2 km), AFT (4.4 km), and AHe (2.8 km).

Material is accreted to the wedge through thrusts slices in the upper plate (frontal accretion) or is offscraped from the
240 subducting plate at depth (underplating). Material motion is constrained by balancing frontal and rearward fluxes, underplating, and erosion. We prescribe a compressional prowedge and an extensional retrowedge, where horizontal velocities decrease along the prowedge and increase along the retrowedge as a function of distance. The vertical rock velocity is also variable with depth, and is defined as the sum of the erosion rate and a component of crustal thickening driven by accretion.

245 The velocities in the model are defined as follows: plate subduction velocity (V_P), prowedge underplating velocity (U_P), prowedge erosional velocity (e_P), and retrowedge erosional velocity (e_R). The plate subduction velocity, or convergence rate, for the Northern Apennines is suggested to be driven entirely by slab rollback, so we used estimates of slab rollback to parameterize the convergence rate. Slab rollback rates are on the order of 6–10 km/My in this region of the Apennines

https://doi.org/10.5194/se-2021-96
Preprint. Discussion started: 10 August 2021

(Faccenna et al., 2014; Rosenbaum and Piana Agostinetti, 2015), so we run the model using these minimum and maximum values as end-member scenarios. We also vary the spatial pattern of erosion rates in the model using two model assumptions: 1) a constant erosion rate across the orogenic wedge (SCR), and 2) a higher erosion rate on the prowedge relative to the retrowedge (VER).

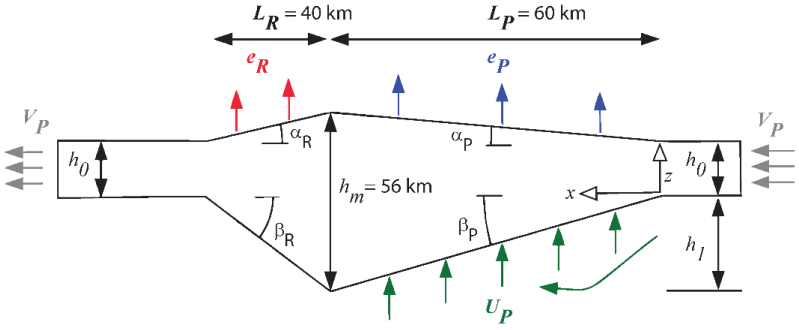

Figure 5 Kinematic model of the Northern Apennines as an orogenic wedge with internal deformation driven by frontal and basal accretion and surface erosion. Mass is balanced to maintain a steady size, and internal deformation is calculated to be consistent with boundary conditions.

3 Results

3.1 Detrital AFT cooling ages

New detrital AFT (8) sample ages are given in Fig. 3b and Tables 6–7. Central ages vary from 5.4 ± 0.6 Ma to 10.5 ± 0.7 Ma, and single grain ages show a wide range of values from 5.1 to 145.3 Ma. All samples except Lima1 show at least two distinct age populations, with minimum age peaks between 5.1 and 8 Ma. All minimum age peaks are younger than the stratigraphic ages of units within the catchment (Cita Sironi et al., 2006; Delfrati et al., 2002; Pialli et al., 2000), with the exception of Magra1. This site contains Plio-Pleistocene deposits exposed in its catchment that are younger than the minimum age peak, but these are locally derived sediments, and the sedimentary bedrock has stratigraphic ages older than the young peak.

In the five southern samples (Serchio, Lima1, Lima2, Pescia and Bisenzio), the youngest peaks represent the largest age populations and are similar to the sample central ages. The three northern samples (Vara, Magra1, Magra2) show two common age populations at 5–6 Ma and at 12–13 Ma and have central ages older than the minimum peak ages, due to a large proportion of older grains.

Table 6 Central Ages and AFT dataset details.

https://doi.org/10.5194/se-2021-96
Preprint. Discussion started: 10 August 2021

Sample	Sampling Site	Lat	Long	Mount Num.	Num. of Grains	ρ_s (x 10^5 cm^{-2})	Ns	ρ_i (x 10^5 cm^{-2})	Ni	ρ_D (x 10^5 cm^{-2})	AFT Central age (Ma)	AFT Central age 1σ (Ma)	P(χ2) (%)	Age disp (%)
Vara	Piana Battolla	44.1950°	9.8569°	1	74	1.13	283	30.7	7672	14.80 ± 0.00	10.53	0.74	0	49
Vara	Piana Battolla	44.1950°	9.8569°	2	76	1.83	432	39.0	9212	15.10 ± 0.01				
Magra2	Pontremoli	44.3873°	9.8868°	1	31	0.94	117	34.5	4285	14.30 ± 0.03	6.94	0.6	0	50
Magra2	Pontremoli	44.3873°	9.8868°	2	69	1.17	220	41.8	7878	14.80 ± 0.03				
Magra1	Isola	44.1867°	9.9258°	1	127	0.95	642	33.9	22978	16.20 ± 0.03	7.81	0.45	0	27
Magra1	Isola	44.1867°	9.9258°	2	23	0.67	72	30.9	3342	15.90 ± 0.03				
Serchio	Piazza al Serchio	44.1920°	10.3016°	1	72	1.36	359	37.2	9834	12.80 ± 0.03	8.08	0.51	0	18
Serchio	Piazza al Serchio	44.1920°	10.3016°	2	28	0.96	78	34.6	2801	13.30 ± 0.03				
Lima2	Cutigliano	44.0907°	10.7596°	1	62	1.00	237	43.1	10202	15.00 ± 0.03	6.63	0.46	0	29
Lima2	Cutigliano	44.0907°	10.7596°	2	38	1.15	152	41.8	5527	14.20 ± 0.04				
Lima1	Borgo a Mozzano	43.9993°	10.5540°	1	31	0.75	97	35.9	4616	14.50 ± 0.03	5.41	0.59	89	0
Bisenzio	Vaiano	43.9277°	11.1258°	1	87	1.02	215	41.2	8992	14.84 ± 0.03	7.09	0.71	0	57
Pescia	Pietrabuona	43.9294°	10.6933°	1	33	1.43	209	42.4	6192	13.80 ± 0.03	8.95	0.69	0	37
Pescia	Pietrabuona	43.9294°	10.6933°	2	44	0.29	242	3.5	6644	13.90 ± 0.03				

ρ_s: spontaneous track density

ρ_i: Induced track density in external detector

ρ_D : induced track density in external detector adjacent to dosimeter glass

Age disp: Age Dispersion

275 **Table 7 Peak Ages with standard error and size of major peaks (%).**

Sample	Sampling Site	Peak Age (Ma) ± 1σ and size of major peaks									
Vara	Piana Battolla	5.9	$^{+1.4}/_{-1.1}$	(35%)	13	$^{+1.0}/_{-0.9}$	(65%)	145.3	$^{+57.3}/_{-41.2}$	(1%)	
Magra2	Pontremoli	5.2	$^{+0.5}/_{-0.5}$	(79%)	13.4	$^{+2.0}/_{-1.8}$	(21%)				
Magra1	Isola	5.1	$^{+1.7}/_{-1.3}$	(28%)	8.2	$^{+0.8}/_{-0.7}$	(60%)	12.3	$^{+13.5}/_{-6.4}$	(12%)	
Serchio	Piazza al Serchio	7.5	$^{+0.5}/_{-0.5}$	(93%)	18.3	$^{+10.3}/_{-6.6}$	(6%)	99.2	$^{+286.5}/_{-74.1}$	(1%)	
Lima2	Cutigliano	6.1	$^{+0.5}/_{-0.4}$	(93%)	17.4	$^{+7.0}/_{-5.0}$	(7%)				
Lima1	Borgo a Mozzano	5.4	$^{+0.6}/_{-0.6}$	(100%)							
Bisenzio	Vaiano	5.3	$^{+0.5}/_{-0.5}$	(90%)	29.4	$^{+7.5}/_{-6.0}$	(10%)				
Pescia	Pietrabuona	8.0	$^{+0.5}/_{-0.5}$	(92%)	24.5	$^{+5.8}/_{-4.7}$	(7%)	111.1	$^{+78.8}/_{-46.3}$	(1%)	

3.2 Geothermal gradients and erosion rates

We report initial geothermal gradients (G_0) and final geothermal gradients (G_f) using the two approaches described in the methods. Given a G_0 = 25 °C/km common to all samples, G_{f_25} ranges from 27.4 to 55.2 °C/km for AHe samples (Table 8)
280 and ranges from 31.2 to 49.7 °C/km for AFT samples (Table 9). Using the second method based on modern heat flow measurements, $G_{0\_heatflow}$ for AHe samples ranges from 9.3 to 42.2 °C/km (Table 8) and ranges from 12.4 to 38.0 °C/km for

https://doi.org/10.5194/se-2021-96
Preprint. Discussion started: 10 August 2021

AFT samples (Table 9). Relative to the G_{f_25}, $G_{f\_heatflow}$ derived from Pauselli et al. (2019) are consistently lower, where all samples lie left of the 1:1 trendline for AHe samples (Fig. 6e) and all but one lie left of the 1:1 trendline for AFT samples (Fig. 6b). In contrast, $G_{f\_heatflow}$ derived from della Vedova et al. (2001) are highly variable, although the majority lie to the right of the 1:1 line for both AHe (Fig. 6e) and AFT (Fig. 6b) samples, indicating that these values are higher relative to G_{f_25}.

Erosion rates calculated using the two methods for estimating geothermal gradients also illustrate different trends for the della Vedova et al. (2001) and Pauselli et al. (2019) heat flow estimates. Erosion rates derived from G_{0_25} plotted against erosion rates derived from della Vedova et al. (2001) $G_{f\_heatflow}$ lie mostly on the 1:1 trendline for both AFT and AHe samples (Fig. 6c,f) and are thus similar. In contrast, erosion rates calculated with Pauselli et al. (2019) $G_{f\_heatflow}$ are lower relative to erosion rates derived from G_{0_25}, but always by a factor of less than two (Fig. 6c,f).

Table 8 Erosion rates and parameters for AHe bedrock samples.

https://doi.org/10.5194/se-2021-96
Preprint. Discussion started: 10 August 2021

Solid Earth
Discussions
Open Access
EGU

						Imposed G_0 = 25 (°C/km)					G_t calculated from heat flow measurements					
ID	Method	Latitude	Longitude	Sample Elevation (km)	Mean Elevation (km)	Inital Geothermal Gradient (°C/km)	Final Geothermal Gradient (°C/km)	Erosion Rate (km/My)	Closure Depth (km)	Closure Temperature (°C)	Inital Geothermal Gradient (°C/km)	Final Geothermal Gradient (°C/km)	Erosion Rate (km/My)	Closure Depth (km)	Closure Temperature (°C)	Heat Flow Measurement Source
020620-3	AHe	44.122	10.068	0.756	0.383	25.0	35.1	0.558	2.2	66.2	29.6	40.0	0.500	1.84	66.7	della Vedova et al. (2001)
03AP08AB	AHe	44.190	10.632	0.880	1.295	25.0	32.4	0.426	2.3	64.0	35.8	42.5	0.282	1.56	63.5	della Vedova et al. (2001)
03AP12A	AHe	44.110	10.735	0.815	1.155	25.0	30.6	0.327	2.1	61.9	40.1	45.0	0.188	1.32	61.3	della Vedova et al. (2001)
03AP23A	AHe	44.129	10.429	0.425	0.709	25.1	27.4	0.144	1.7	53.6	19.7	40.0	0.188	2.15	52.9	della Vedova et al. (2001)
03AP23B	AHe	44.129	10.429	0.425	0.709	25.0	29	0.241	2.0	59.6	36.4	40.0	0.156	1.34	59.2	della Vedova et al. (2001)
03AP28A	AHe	44.111	10.529	1.035	0.899	25.0	30.1	0.302	2.1	61.0	34.8	40.0	0.229	1.49	61.5	della Vedova et al. (2001)
03AP28C	AHe	44.111	10.529	1.035	0.899	25.0	29.3	0.262	2.0	59.8	35.5	40.0	0.194	1.43	60.3	della Vedova et al. (2001)
03AP28D	AHe	44.111	10.529	1.035	0.899	25.0	30.5	0.325	2.1	61.6	34.3	40.0	0.250	1.53	61.9	della Vedova et al. (2001)
03AP29A	AHe	44.130	10.542	1.320	1.050	25.0	31.9	0.399	2.2	63.4	32.7	40.0	0.326	1.67	63.6	della Vedova et al. (2001)
03AP31A	AHe	44.142	10.553	1.815	1.131	25.0	31	0.353	2.1	62.0	33.4	40.0	0.293	1.62	62.6	della Vedova et al. (2001)
03AP31B	AHe	44.142	10.553	1.815	1.131	25.1	33.6	0.487	2.3	64.9	33.1	42.5	0.411	1.72	65.5	della Vedova et al. (2001)
03AP34	AHe	44.066	10.107	0.285	0.340	25.1	29.1	0.244	1.9	59.6	36.0	40.0	0.172	1.31	59.7	della Vedova et al. (2001)
03AP51	AHe	44.014	10.380	1.060	0.688	25.0	30.4	0.322	2.0	61.5	34.2	40.0	0.256	1.50	62.0	della Vedova et al. (2001)
03AP51C	AHe	44.014	10.380	1.060	0.688	25.0	29.7	0.279	2.0	60.1	35.0	40.0	0.218	1.43	60.9	della Vedova et al. (2001)
03AP52A	AHe	44.084	10.463	0.370	0.582	25.1	28.7	0.222	1.9	58.8	36.6	40.0	0.146	1.30	58.6	della Vedova et al. (2001)
03AP52B	AHe	44.084	10.463	0.370	0.582	25.0	28.7	0.223	1.9	58.8	36.6	40.0	0.147	1.30	58.7	della Vedova et al. (2001)
03AP52C	AHe	44.084	10.463	0.370	0.582	25.0	28.2	0.194	1.9	57.7	37.1	40.0	0.125	1.25	57.5	della Vedova et al. (2001)
03GB07	AHe	44.124	10.059	0.675	0.356	25.0	32	0.402	2.0	63.4	32.7	40.0	0.333	1.58	63.9	della Vedova et al. (2001)
03GB09	AHe	44.162	10.115	0.335	0.546	25.0	32.5	0.432	2.1	64.2	35.2	42.5	0.307	1.50	64.0	della Vedova et al. (2001)
03GB10	AHe	44.177	10.156	0.530	0.656	25.0	29.4	0.265	2.0	60.1	38.2	42.5	0.172	1.29	60.1	della Vedova et al. (2001)
03RE02	AHe	44.148	10.438	0.765	0.836	25.0	29.3	0.258	2.0	59.9	35.8	40.0	0.182	1.40	60.0	della Vedova et al. (2001)
03RE05A	AHe	44.188	10.480	1.495	1.138	25.1	30.8	0.336	2.1	61.7	34.0	40.0	0.269	1.59	62.4	della Vedova et al. (2001)
03RE05B	AHe	44.188	10.480	1.495	1.138	25.1	31.8	0.392	2.2	63.2	32.8	40.0	0.322	1.68	63.6	della Vedova et al. (2001)
03RE05C	AHe	44.188	10.480	1.495	0.582	25.0	30.7	0.342	2.0	61.5	36.0	42.5	0.278	1.44	62.8	della Vedova et al. (2001)
03RE05CD	AHe	44.188	10.480	1.495	1.138	25.0	29	0.243	2.0	58.0	35.7	40.0	0.185	1.42	59.1	della Vedova et al. (2001)
03RE05D	AHe	44.188	10.480	1.495	0.582	25.0	32.4	0.427	2.1	63.6	34.2	42.5	0.360	1.56	64.7	della Vedova et al. (2001)
03RE06A	AHe	44.201	10.488	1.640	1.194	25.0	31.9	0.395	2.2	63.0	35.1	42.5	0.313	1.59	63.8	della Vedova et al. (2001)
03RE06B	AHe	44.201	10.488	1.640	1.194	25.0	31.3	0.367	2.2	62.4	35.7	42.5	0.286	1.54	63.3	della Vedova et al. (2001)
03RE12A	AHe	44.059	10.767	0.460	0.942	25.0	28.8	0.229	2.0	59.2	42.2	45.0	0.104	1.14	57.5	della Vedova et al. (2001)
03RE12B	AHe	44.059	10.767	0.460	0.942	25.0	29	0.243	2.0	59.6	42.0	45.0	0.112	1.16	57.9	della Vedova et al. (2001)
03RE14A	AHe	44.005	10.665	0.840	0.635	25.0	31.5	0.377	2.1	62.9	33.2	40.0	0.303	1.58	63.2	della Vedova et al. (2001)
03RE14B	AHe	44.005	10.665	0.840	0.635	25.0	27.9	0.184	1.6	51.7	36.7	40.0	0.139	1.18	54.3	della Vedova et al. (2001)
03RE20	AHe	44.098	10.326	1.055	0.808	25.0	32.5	0.432	2.2	64.1	32.1	40.0	0.358	1.69	64.3	della Vedova et al. (2001)
03RE7	AHe	44.200	10.676	1.600	1.214	25.0	38.6	0.727	2.4	68.7	30.7	45.0	0.639	1.99	69.1	della Vedova et al. (2001)
03RE7R1	AHe	44.200	10.676	1.600	1.214	25.0	37.5	0.676	2.4	68.0	31.7	45.0	0.581	1.90	68.5	della Vedova et al. (2001)
03TH02	AHe	44.086	10.568	0.979	0.881	25.0	29.9	0.291	2.0	60.7	37.5	42.5	0.206	1.37	61.2	della Vedova et al. (2001)
03TH02B	AHe	44.086	10.568	0.979	0.881	25.0	29.3	0.261	2.0	59.8	38.1	42.5	0.181	1.33	60.3	della Vedova et al. (2001)
03TH12B	AHe	44.080	10.600	0.678	0.904	25.1	31.4	0.371	2.1	63.0	33.8	40.0	0.273	1.57	62.7	della Vedova et al. (2001)
03TH13A	AHe	44.013	10.593	0.153	0.578	25.0	27.6	0.160	1.8	56.4	16.0	40.0	0.273	2.82	56.5	della Vedova et al. (2001)
03TH13C	AHe	44.013	10.593	0.153	0.578	25.0	28	0.182	1.8	57.4	37.6	40.0	0.102	1.20	56.4	della Vedova et al. (2001)
03TH18A	AHe	43.980	10.552	0.047	0.449	25.1	28.3	0.197	1.8	58.0	37.3	40.0	0.114	1.22	57.2	della Vedova et al. (2001)
03TH23A	AHe	44.124	10.628	1.645	1.205	25.0	33.6	0.485	2.3	64.9	33.3	42.5	0.400	1.72	65.4	della Vedova et al. (2001)
03TH23BD	AHe	44.124	10.628	1.645	1.205	25.1	32.6	0.431	2.2	63.8	34.3	42.5	0.347	1.64	64.4	della Vedova et al. (2001)
03TH23C	AHe	44.124	10.628	1.645	1.205	25.0	33.9	0.502	2.3	65.1	33.0	42.5	0.418	1.75	65.8	della Vedova et al. (2001)
050320-1C	AHe	44.263	10.664	1.112	1.024	25.0	51.7	1.255	2.6	74.7	17.8	42.5	1.533	3.68	74.4	della Vedova et al. (2001)
050320-1D	AHe	44.263	10.664	1.112	1.024	25.0	42.5	0.896	2.5	70.8	25.0	42.5	0.896	2.48	70.8	della Vedova et al. (2001)
050320-2B	AHe	44.276	10.674	1.239	0.965	25.0	31.9	0.401	2.2	63.3	35.2	42.5	0.311	1.55	63.9	della Vedova et al. (2001)
050320-2C	AHe	44.276	10.674	1.239	0.965	25.0	31.7	0.392	2.2	63.1	35.4	42.5	0.302	1.54	63.8	della Vedova et al. (2001)
050320-3A	AHe	44.280	10.668	1.272	0.957	25.0	28.9	0.237	2.0	58.2	38.3	42.5	0.171	1.30	59.3	della Vedova et al. (2001)
050320-3B	AHe	44.280	10.668	1.272	0.957	25.0	31.2	0.360	2.1	62.3	35.9	42.5	0.276	1.50	63.0	della Vedova et al. (2001)
050320-3C	AHe	44.280	10.668	1.272	0.957	25.0	30.6	0.331	2.1	61.6	36.5	42.5	0.249	1.45	62.4	della Vedova et al. (2001)
1926	AHe	44.107	11.729	0.250	0.471	25.1	29.2	0.249	1.9	59.8	21.3	25.5	0.295	2.26	59.9	Pauselli et al. (2019)
1926B	AHe	44.107	11.729	0.250	0.471	25.0	33.2	0.467	2.1	64.8	17.2	25.5	0.650	3.08	64.9	Pauselli et al. (2019)
1926C	AHe	44.107	11.729	0.250	0.471	25.0	29.4	0.260	1.9	60.1	21.1	25.5	0.311	2.30	60.1	Pauselli et al. (2019)
1926D	AHe	44.107	11.729	0.250	0.471	25.0	34	0.504	2.1	65.6	16.5	25.5	0.723	3.25	65.6	Pauselli et al. (2019)
1929	AHe	44.037	11.504	0.700	0.702	25.0	42.9	0.910	2.4	71.1	12.6	28.5	1.431	4.78	70.7	Pauselli et al. (2019)
AP1	AHe	43.790	12.146	0.700	0.776	25.0	45.7	1.022	2.5	72.3	15.1	23.5	1.431	4.12	72.3	Pauselli et al. (2019)
AP17	AHe	43.876	12.110	0.600	0.605	25.0	40.2	0.800	2.4	69.8	9.4	22.5	1.539	6.17	69.1	Pauselli et al. (2019)
AP2	AHe	43.789	12.151	0.600	0.771	25.0	36.4	0.622	2.3	67.4	13.1	24.0	1.033	4.36	67.4	Pauselli et al. (2019)
AP3	AHe	43.815	12.149	0.900	0.727	25.0	35.4	0.575	2.2	66.5	14.1	23.5	0.867	3.95	65.9	Pauselli et al. (2019)
AP30	AHe	43.895	11.779	0.750	0.879	25.0	42	0.873	2.4	70.7	12.0	27.5	1.454	5.07	70.6	Pauselli et al. (2019)
AP33	AHe	43.919	11.792	0.650	0.801	25.0	45.3	1.011	2.5	72.3	9.3	27.0	1.921	6.64	72.1	Pauselli et al. (2019)
AP36E	AHe	44.097	11.955	0.370	0.271	25.0	28.1	0.189	1.7	56.3	19.4	22.5	0.236	2.20	55.6	Pauselli et al. (2019)
AP37	AHe	44.015	11.951	0.150	0.423	25.0	33.4	0.478	2.1	65.1	12.5	21.0	0.870	4.24	65.2	Pauselli et al. (2019)
AP38	AHe	43.797	11.914	1.200	0.858	25.0	43.6	0.947	2.5	71.5	10.9	26.0	1.533	5.55	70.2	Pauselli et al. (2019)
AP43R1	AHe	43.818	11.733	0.515	0.860	25.1	33.1	0.458	2.2	64.8	21.3	29.5	0.537	2.58	64.8	Pauselli et al. (2019)
AP43R2	AHe	43.818	11.733	0.515	0.860	25.1	32.5	0.425	2.2	64.1	22.0	29.5	0.485	2.48	64.3	Pauselli et al. (2019)
AP44R1	AHe	43.824	11.746	0.725	0.868	25.0	38.7	0.735	2.4	69.1	16.2	29.5	1.017	3.64	68.9	Pauselli et al. (2019)
AP45R1	AHe	43.844	11.749	0.940	0.897	25.0	35.3	0.568	2.3	66.5	19.5	29.5	0.687	2.90	66.3	Pauselli et al. (2019)
AP45R2	AHe	43.844	11.749	0.940	0.897	25.0	53.1	1.304	2.6	75.1	NA	29.0	0.687	0.99	75.7	Pauselli et al. (2019)

https://doi.org/10.5194/se-2021-96
Preprint. Discussion started: 10 August 2021

AP47R1	AHe	43.864	11.739	1.365	0.906	25.0	42	0.873	2.4	70.6	14.5	29.0	1.200	4.15	69.7	Pauselli et al. (2019)
AP48R1	AHe	43.879	11.711	1.655	0.907	25.0	38.8	0.736	2.4	68.9	17.7	30.0	0.893	3.30	67.9	Pauselli et al. (2019)
AP48R2	AHe	43.879	11.711	1.655	0.907	25.0	38.8	0.736	2.4	68.9	17.7	30.0	0.893	3.30	67.9	Pauselli et al. (2019)
AP5	AHe	44.189	11.501	0.200	0.521	25.0	29	0.241	1.9	59.6	24.5	28.5	0.247	1.96	59.6	della Vedova et al. (2001)
AP52	AHe	43.905	11.791	0.565	0.836	25.1	38.2	0.706	2.3	68.7	13.7	26.5	1.141	4.32	68.9	Pauselli et al. (2019)
AP53	AHe	43.934	11.656	0.907	0.830	25.0	31.1	0.356	2.1	62.5	23.0	29.0	0.383	2.28	62.4	Pauselli et al. (2019)
AP54	AHe	43.961	11.670	0.690	0.811	25.0	39.5	0.765	2.4	69.4	13.9	27.5	1.176	4.26	69.1	Pauselli et al. (2019)
AP55	AHe	44.013	11.687	1.070	0.722	25.0	42.7	0.901	2.4	70.9	12.7	27.5	1.347	4.69	69.9	Pauselli et al. (2019)
AP57	AHe	43.995	11.719	0.450	0.746	25.0	42.9	0.910	2.4	71.2	10.8	27.5	1.669	5.68	71.5	Pauselli et al. (2019)
AP5B	AHe	44.189	11.501	0.200	0.521	25.0	36.1	0.610	2.2	67.3	17.3	28.5	0.841	3.24	67.6	della Vedova et al. (2001)
AP5C	AHe	44.189	11.501	0.200	0.521	25.0	46.5	1.057	2.4	72.8	32.9	28.5	0.841	1.86	72.6	della Vedova et al. (2001)
AP5D	AHe	44.189	11.501	0.200	0.521	25.0	33.9	0.501	2.2	65.5	19.5	28.5	0.634	2.78	65.7	della Vedova et al. (2001)
AP8	AHe	44.147	11.449	0.300	0.629	25.1	42.7	0.903	2.4	71.2	12.9	30.0	1.483	4.69	71.4	della Vedova et al. (2001)
AP9	AHe	44.115	11.431	0.400	0.674	25.0	42.5	0.893	2.4	71.0	11.1	27.5	1.601	5.43	71.3	Pauselli et al. (2019)
C1	AHe	44.113	11.002	0.500	0.765	25.0	32.2	0.415	2.1	63.9	33.0	40.0	0.312	1.62	63.6	della Vedova et al. (2001)
C10	AHe	44.143	11.191	0.605	0.766	25.0	55.2	1.386	2.6	76.0	NA	35.0	0.312	0.49	73.3	della Vedova et al. (2001)
C11	AHe	44.001	10.807	0.950	0.667	25.1	30.9	0.342	2.0	62.0	38.7	45.0	0.247	1.34	62.8	della Vedova et al. (2001)
C13	AHe	44.021	10.864	0.700	0.747	25.0	32.8	0.443	2.2	64.3	39.7	47.5	0.295	1.37	64.6	della Vedova et al. (2001)
C16	AHe	44.060	10.913	0.630	0.909	25.0	34.1	0.513	2.2	65.6	36.2	45.0	0.353	1.54	65.3	della Vedova et al. (2001)
C17	AHe	44.068	10.919	0.625	0.921	25.0	34.2	0.517	2.3	65.8	36.2	45.0	0.355	1.54	65.3	della Vedova et al. (2001)
C2	AHe	44.004	11.012	0.830	0.660	25.0	34.4	0.522	2.2	65.7	35.1	45.0	0.406	1.57	66.1	della Vedova et al. (2001)
C22	AHe	44.041	10.932	0.850	0.821	25.1	33	0.454	2.2	64.6	36.8	45.0	0.330	1.49	64.8	della Vedova et al. (2001)
C23	AHe	44.021	10.929	0.884	0.719	25.0	32.9	0.453	2.2	64.6	36.7	45.0	0.338	1.49	65.0	della Vedova et al. (2001)
C29	AHe	44.731	9.386	0.320	0.775	25.0	32.9	0.454	2.2	64.7	27.2	35.0	0.412	2.00	64.5	della Vedova et al. (2001)
C3	AHe	44.014	11.025	0.780	0.706	25.0	33	0.452	2.2	64.4	36.7	45.0	0.331	1.48	64.8	della Vedova et al. (2001)
C34	AHe	44.417	9.949	0.510	0.855	25.1	34.1	0.508	2.2	65.7	31.2	40.0	0.405	1.78	65.3	della Vedova et al. (2001)
C37	AHe	44.246	10.683	0.641	1.064	25.0	39.3	0.755	2.4	69.3	31.2	45.0	0.610	1.93	69.0	della Vedova et al. (2001)
C4	AHe	44.028	11.038	0.680	0.753	25.1	39.7	0.772	2.4	69.5	28.7	43.5	0.696	2.06	69.6	della Vedova et al. (2001)
C40	AHe	44.223	10.758	1.250	0.980	25.1	45.5	1.017	2.5	72.3	25.4	46.0	1.007	2.48	72.2	della Vedova et al. (2001)
C5	AHe	44.049	11.044	0.610	0.798	25.0	32.6	0.434	2.2	64.2	35.0	42.5	0.313	1.54	64.0	della Vedova et al. (2001)
C52A	AHe	44.013	11.503	0.360	0.661	25.1	32.4	0.419	2.1	63.9	21.1	28.5	0.497	2.53	64.1	Pauselli et al. (2019)
C6	AHe	44.095	11.044	0.650	0.779	25.0	39.5	0.762	2.4	69.3	25.5	40.0	0.751	2.32	69.3	della Vedova et al. (2001)
C7	AHe	44.111	11.039	0.625	0.755	25.0	38.5	0.725	2.3	68.9	26.4	40.0	0.693	2.22	68.8	della Vedova et al. (2001)
C8	AHe	44.115	11.204	0.700	0.757	25.0	40.3	0.802	2.4	69.8	22.4	37.5	0.870	2.66	69.8	della Vedova et al. (2001)
C9	AHe	44.106	11.204	1.000	0.738	25.0	46.3	1.051	2.5	72.7	18.0	37.5	1.275	3.44	72.4	della Vedova et al. (2001)
CIM1	AHe	44.194	10.699	2.165	1.174	25.0	40.2	0.800	2.5	69.5	28.9	45.0	0.745	2.14	70.0	della Vedova et al. (2001)
CIM1R1	AHe	44.194	10.699	2.165	1.174	25.0	40.2	0.802	2.5	69.5	28.9	45.0	0.748	2.14	70.1	della Vedova et al. (2001)
CIM2	AHe	44.194	10.704	2.045	1.165	25.1	42.8	0.908	2.5	71.0	26.8	45.0	0.879	2.35	71.2	della Vedova et al. (2001)
CIM3	AHe	44.196	10.692	1.950	1.184	25.1	42.7	0.903	2.5	70.9	26.9	45.0	0.871	2.34	71.1	della Vedova et al. (2001)
CIM3R1	AHe	44.196	10.692	1.950	1.184	25.0	38.1	0.705	2.4	68.3	30.8	45.0	0.629	1.97	68.7	della Vedova et al. (2001)
CIM4	AHe	44.200	10.684	1.830	1.196	25.0	40.4	0.810	2.5	69.8	28.8	45.0	0.749	2.15	70.0	della Vedova et al. (2001)
CIM4R1	AHe	44.200	10.684	1.830	1.196	25.0	39.7	0.779	2.5	69.3	29.5	45.0	0.710	2.09	69.8	della Vedova et al. (2001)
CIM5	AHe	44.202	10.677	1.750	1.208	25.0	39.2	0.751	2.4	69.0	30.0	45.0	0.675	2.04	69.2	della Vedova et al. (2001)
CIM5A	AHe	44.202	10.677	1.750	1.208	25.0	40.6	0.818	2.5	70.0	28.7	45.0	0.756	2.16	70.1	della Vedova et al. (2001)
CIM5R1	AHe	44.202	10.677	1.750	1.208	25.1	41.7	0.857	2.5	70.4	27.9	45.0	0.808	2.25	70.7	della Vedova et al. (2001)
CIM6	AHe	44.201	10.666	1.660	1.230	25.0	40.2	0.800	2.5	69.7	29.2	45.0	0.730	2.13	70.0	della Vedova et al. (2001)
CIM6R1	AHe	44.201	10.666	1.660	1.230	25.0	39.9	0.785	2.5	69.4	29.4	45.0	0.712	2.10	69.8	della Vedova et al. (2001)
VALD10a	AHe	43.653	11.640	1.400	0.836	25.0	36.9	0.651	2.3	67.7	17.7	28.5	0.804	3.22	67.1	Pauselli et al. (2019)
VALD1a	AHe	43.594	11.603	0.497	0.471	25.0	29.3	0.259	1.9	59.9	24.7	29.0	0.262	1.95	59.9	Pauselli et al. (2019)
VALD2a	AHe	43.612	11.645	0.500	0.685	25.0	32	0.405	2.1	63.7	23.0	30.0	0.438	2.31	63.7	Pauselli et al. (2019)
VALD2R1	AHe	43.612	11.645	0.500	0.685	25.0	32	0.408	2.1	63.7	23.0	30.0	0.441	2.31	63.8	Pauselli et al. (2019)
VALD4a1	AHe	43.620	11.648	0.740	0.730	25.0	33.8	0.497	2.2	65.4	20.8	29.5	0.575	2.63	65.2	Pauselli et al. (2019)
VALD4a2	AHe	43.620	11.648	0.740	0.730	25.0	31.2	0.359	2.1	62.5	23.3	29.5	0.381	2.23	62.4	Pauselli et al. (2019)
VALD4R1	AHe	43.620	11.648	0.740	0.730	25.1	32.8	0.442	2.1	64.3	21.8	29.5	0.495	2.46	64.2	Pauselli et al. (2019)
VALD5a	AHe	43.621	11.656	0.850	0.747	25.0	33.3	0.470	2.2	64.8	21.9	30.0	0.523	2.48	64.7	Pauselli et al. (2019)
VALD5R1	AHe	43.621	11.656	0.850	0.747	25.0	33.4	0.474	2.2	64.8	21.8	30.0	0.529	2.50	64.7	Pauselli et al. (2019)
VALD6a	AHe	43.620	11.659	0.880	0.746	25.0	33.1	0.465	2.2	64.7	22.0	30.0	0.513	2.46	64.5	Pauselli et al. (2019)
VALD6R1	AHe	43.620	11.659	0.880	0.746	25.0	33.6	0.490	2.2	65.2	21.5	30.0	0.548	2.54	64.9	Pauselli et al. (2019)
VALD7a	AHe	43.604	11.651	1.100	0.658	25.0	35.3	0.575	2.2	66.5	21.0	31.0	0.642	2.63	66.1	Pauselli et al. (2019)
VALD8R1	AHe	43.626	11.684	1.200	0.782	25.0	34.5	0.528	2.2	65.6	21.4	30.5	0.587	2.58	65.4	Pauselli et al. (2019)
VALD8R2	AHe	43.626	11.684	1.200	0.782	25.0	36.2	0.615	2.3	67.1	19.9	30.5	0.712	2.84	66.8	Pauselli et al. (2019)

Kinetic Parameters for (U-Th)/He apatite *(from Farley, 2000 and Reiners and Brandon, 2006)*

E_a = 138 kJ mol^{-1} (activation energy)

a_s = 45 µm (effective spherical radius for the diffusion domain)

Ω = 1.36 x 10^6 (frequency factor calculated as 55D_0a^{-2})

$t_{c,10}$ = 62.7°C (effective closure temperature for 10 Myr^{-1} cooling rates and specified a_s value)

Table 9 Erosion rates and parameters for AFT bedrock samples.

https://doi.org/10.5194/se-2021-96
Preprint. Discussion started: 10 August 2021

Solid Earth
Discussions
Open Access
EGU

						Imposed G_0 = 25 (°C/km)					G_r calculated from heat flow measurements					
ID	Method	Latitude	Longitude	Sample Elevation (km)	Mean Elevation (km)	Inital Geothermal Gradient (°C/km)	Final Geothermal Gradient (°C/km)	Erosion Rate (km/My)	Closure Depth (km)	Closure Temperature (°C)	Inital Geothermal Gradient (°C/km)	Final Geothermal Gradient (°C/km)	Erosion Rate (km/My)	Closure Depth (km)	Closure Temperature (°C)	Heat Flow Measurement Source
1927	AFT	44.064	11.597	0.350	0.667	25.1	32.2	0.410	4.1	113.9	20.8	28.0	0.494	4.9	113.4	Pauselli et al. (2019)
1929	AFT	44.037	11.504	0.700	0.619	25.0	35.3	0.574	4.3	118.8	18.3	28.5	0.743	5.8	117.9	Pauselli et al. (2019)
1930	AFT	44.069	11.492	1.150	0.630	25.0	40.4	0.805	4.5	123.2	14.8	29.0	1.155	7.5	121.8	Pauselli et al. (2019)
03GB07	AFT	44.124	10.059	0.675	0.356	25.0	34.1	0.508	4.2	116.3	30.8	40.0	0.429	3.4	117.2	della Vedova et al. (2001)
03RE20	AFT	44.098	10.326	1.055	0.760	25.0	34.6	0.536	4.3	117.1	30.2	40.0	0.459	3.6	117.7	della Vedova et al. (2001)
050320-1a	AFT	44.263	10.664	1.112	0.976	25.0	34.5	0.532	4.3	117.4	32.9	42.5	0.422	3.3	118.1	della Vedova et al. (2001)
050320-1b	AFT	44.263	10.664	1.112	0.976	25.0	38.3	0.712	4.5	121.7	29.1	42.5	0.634	3.9	122.0	della Vedova et al. (2001)
AP 10	AFT	44.121	11.396	0.500	0.685	25.0	39.8	0.780	4.5	123.2	13.2	27.5	1.277	8.5	121.9	Pauselli et al. (2019)
Ap 15	AFT	43.819	11.952	0.700	0.805	25.0	32.1	0.411	4.1	112.4	22.9	30.0	0.446	4.4	111.8	Pauselli et al. (2019)
AP 34	AFT	44.097	11.315	0.600	0.653	25.0	35.7	0.592	4.3	119.3	17.4	28.0	0.802	6.2	118.3	Pauselli et al. (2019)
AP 43	AFT	43.818	11.733	0.515	0.805	25.0	36	0.608	4.4	119.9	18.4	29.5	0.793	5.9	119.2	Pauselli et al. (2019)
AP 44	AFT	43.824	11.746	0.725	0.807	25.0	38.6	0.725	4.5	122.0	16.7	30.0	0.996	6.7	121.3	Pauselli et al. (2019)
AP 45	AFT	43.828	11.749	0.940	0.809	25.0	38.9	0.741	4.5	122.3	16.1	29.5	1.031	6.9	121.0	Pauselli et al. (2019)
AP 47	AFT	43.864	11.739	1.365	0.816	25.0	40.6	0.816	4.5	123.1	14.6	29.0	1.176	7.6	121.4	Pauselli et al. (2019)
AP 52	AFT	43.905	11.723	0.565	0.799	25.1	36.7	0.633	4.4	120.1	18.4	30.0	0.824	6.0	119.7	Pauselli et al. (2019)
AP 53	AFT	43.934	11.656	0.907	0.814	25.0	33.1	0.458	4.2	114.5	21.0	29.0	0.536	4.9	113.9	Pauselli et al. (2019)
AP 54	AFT	43.961	11.670	0.690	0.747	25.0	36.3	0.617	4.4	119.8	17.4	28.5	0.835	6.3	119.1	Pauselli et al. (2019)
AP 55	AFT	44.013	11.687	1.070	0.672	25.0	34.4	0.525	4.2	116.6	19.3	28.5	0.648	5.4	115.5	Pauselli et al. (2019)
AP 56	AFT	43.983	11.686	0.500	0.723	25.0	39	0.747	4.5	122.4	14.7	28.5	1.134	7.6	121.8	Pauselli et al. (2019)
AP 57	AFT	43.995	11.719	0.450	0.688	25.0	40.6	0.814	4.5	123.5	12.4	27.5	1.384	9.0	122.5	Pauselli et al. (2019)
AP 9	AFT	44.115	11.431	0.400	0.673	25.0	39.4	0.761	4.5	122.8	13.9	28.0	1.211	8.0	122.0	Pauselli et al. (2019)
BOR2	AFT	44.435	9.425	0.452	0.779	25.0	33	0.457	4.2	115.9	32.2	40.0	0.355	3.3	116.2	della Vedova et al. (2001)
BORl	AFT	44.435	9.425	0.450	0.779	25.0	34.2	0.519	4.3	117.8	30.9	40.0	0.422	3.5	117.8	della Vedova et al. (2001)
BT1	AFT	44.085	9.787	0.475	0.104	25.0	39.8	0.780	4.4	123.0	25.2	40.0	0.775	4.3	122.6	della Vedova et al. (2001)
BT2	AFT	44.085	9.787	0.525	0.104	25.0	39.6	0.770	4.4	122.6	25.4	40.0	0.762	4.3	122.5	della Vedova et al. (2001)
C1	AFT	44.113	11.002	0.500	0.789	25.0	34	0.505	4.3	117.1	33.7	42.5	0.379	3.2	117.5	della Vedova et al. (2001)
C10	AFT	44.143	11.191	0.605	0.683	25.0	40.3	0.802	4.5	123.3	19.9	35.0	0.954	5.6	122.9	della Vedova et al. (2001)
C11	AFT	44.001	10.807	0.950	0.644	25.1	32.2	0.414	3.8	106.7	37.4	45.0	0.299	2.7	110.7	della Vedova et al. (2001)
C13	AFT	44.021	10.864	0.700	0.731	25.0	34.6	0.533	4.3	117.6	38.0	47.5	0.369	2.8	118.6	della Vedova et al. (2001)
C16	AFT	44.060	10.913	0.630	0.807	25.0	45.3	1.014	4.7	126.6	24.7	45.0	1.022	4.7	126.5	della Vedova et al. (2001)
C17	AFT	44.068	10.919	0.625	0.818	25.0	37.2	0.661	4.4	121.0	32.9	45.0	0.522	3.4	121.2	della Vedova et al. (2001)
C2	AFT	44.004	11.012	0.830	0.548	25.0	35.8	0.593	4.3	118.9	33.9	45.0	0.466	3.2	119.5	della Vedova et al. (2001)
C22	AFT	44.041	10.932	0.850	0.747	25.0	45.3	1.012	4.6	126.7	24.7	45.0	1.020	4.7	126.4	della Vedova et al. (2001)
C23	AFT	44.021	10.929	0.884	0.689	25.1	38	0.692	4.4	121.0	32.7	46.0	0.563	3.4	121.6	della Vedova et al. (2001)
C29	AFT	44.731	9.386	0.320	0.804	25.0	36.5	0.630	4.4	120.4	23.4	35.0	0.668	4.7	120.2	della Vedova et al. (2001)
C3	AFT	44.014	11.025	0.780	0.580	25.1	38.4	0.711	4.4	121.4	30.0	43.5	0.621	3.7	122.2	della Vedova et al. (2001)
C34	AFT	44.417	9.949	0.510	0.820	25.1	32.2	0.410	4.1	113.8	33.1	40.0	0.309	3.2	114.4	della Vedova et al. (2001)
C37	AFT	44.246	10.683	0.641	1.016	25.0	44.8	0.991	4.7	126.6	23.7	43.5	1.032	4.9	126.3	della Vedova et al. (2001)
C38	AFT	44.223	10.777	0.980	0.950	25.0	44.5	0.977	4.7	125.9	26.0	45.5	0.952	4.5	126.2	della Vedova et al. (2001)
C4	AFT	44.028	11.038	0.680	0.620	25.0	43.4	0.933	4.6	125.5	25.1	43.5	0.930	4.6	125.5	della Vedova et al. (2001)
C40	AFT	44.223	10.758	1.250	0.977	25.0	41.5	0.851	4.6	123.8	29.2	46.0	0.763	3.9	124.4	della Vedova et al. (2001)
C5	AFT	44.049	11.044	0.610	0.679	25.0	36	0.606	4.4	119.6	32.4	43.5	0.484	3.4	120.0	della Vedova et al. (2001)
C52	AFT	44.013	11.503	0.360	0.594	25.0	35.1	0.562	4.3	118.8	18.4	28.5	0.739	5.8	118.3	Pauselli et al. (2019)
C6	AFT	44.095	11.044	0.650	0.735	25.0	37.3	0.669	4.4	120.9	27.6	40.0	0.614	4.0	121.0	della Vedova et al. (2001)
C7	AFT	44.111	11.039	0.625	0.738	25.0	36.4	0.626	4.4	120.1	28.5	40.0	0.558	3.8	120.2	della Vedova et al. (2001)
C8	AFT	44.115	11.207	0.700	0.680	25.0	35.5	0.580	4.3	118.8	27.0	37.5	0.544	4.0	119.1	della Vedova et al. (2001)
C9	AFT	44.106	11.204	1.000	0.673	27.0	36.8	0.512	4.0	117.7	27.7	37.5	0.502	3.9	117.9	della Vedova et al. (2001)
CAS1	AFT	44.206	10.446	1.300	1.061	25.0	33.2	0.466	4.2	113.9	31.7	40.0	0.380	3.4	115.0	della Vedova et al. (2001)
CAS2	AFT	44.174	10.424	0.965	0.980	25.1	32.4	0.424	4.1	112.6	32.7	40.0	0.331	3.2	113.7	della Vedova et al. (2001)
CAST2	AFT	44.105	10.415	0.270	0.811	25.0	31.4	0.372	4.1	112.2	34.0	40.0	0.264	3.0	113.0	della Vedova et al. (2001)
CAST3	AFT	44.105	10.415	0.240	0.811	25.1	31.9	0.395	4.1	113.9	33.5	40.0	0.285	3.1	114.0	della Vedova et al. (2001)
CB3	AFT	44.051	9.830	0.000	0.079	25.0	32.8	0.443	4.0	115.1	32.3	40.0	0.350	3.2	115.7	della Vedova et al. (2001)
CB4	AFT	44.051	9.830	0.000	0.079	25.1	32.5	0.428	4.0	114.5	32.6	40.0	0.334	3.1	115.0	della Vedova et al. (2001)
CB5	AFT	44.051	9.830	0.000	0.079	24.9	33.7	0.493	4.1	116.7	31.3	40.0	0.402	3.3	117.3	della Vedova et al. (2001)
CH1	AFT	43.601	11.411	0.303	0.337	25.0	36.1	0.611	4.3	119.7	23.9	35.0	0.634	4.5	119.8	Pauselli et al. (2019)
CH2	AFT	43.541	11.430	0.504	0.379	25.0	35.8	0.596	4.3	119.2	29.1	40.0	0.526	3.7	119.7	Pauselli et al. (2019)
CH3	AFT	43.565	11.382	0.722	0.373	25.0	35.3	0.571	4.2	118.2	28.1	38.5	0.521	3.8	118.7	Pauselli et al. (2019)
CH4	AFT	43.562	11.380	0.857	0.376	25.1	35.1	0.556	4.2	117.7	28.4	38.5	0.506	3.7	118.3	Pauselli et al. (2019)
CIM1	AFT	44.194	10.699	2.165	1.121	25.0	36.7	0.637	4.4	118.9	32.5	45.0	0.533	3.4	119.8	della Vedova et al. (2001)
CIM2	AFT	44.194	10.704	2.045	1.116	25.0	36	0.603	4.4	118.0	33.4	45.0	0.494	3.3	119.3	della Vedova et al. (2001)
CIM3	AFT	44.196	10.692	1.950	1.124	25.0	36.2	0.616	4.4	118.5	33.2	45.0	0.504	3.4	119.8	della Vedova et al. (2001)
CIM4	AFT	44.200	10.684	1.830	1.128	25.0	37	0.652	4.4	119.7	30.1	42.5	0.571	3.7	120.2	della Vedova et al. (2001)
CIM5	AFT	44.202	10.677	1.750	1.134	25.1	36	0.603	4.4	118.8	33.0	44.5	0.490	3.4	119.4	della Vedova et al. (2001)
CIM6	AFT	44.201	10.666	1.660	1.149	25.1	36.6	0.632	4.4	119.6	32.0	44.0	0.526	3.5	120.2	della Vedova et al. (2001)
GOM2	AFT	44.125	10.642	1.850	1.061	25.0	33.9	0.498	4.1	112.0	34.6	44.0	0.392	3.1	114.6	della Vedova et al. (2001)
GOM3	AFT	44.134	10.656	1.300	1.096	25.0	36.3	0.618	4.4	119.4	32.5	44.0	0.501	3.4	120.0	della Vedova et al. (2001)
MG3	AFT	44.235	9.472	0.000	0.193	25.0	31.2	0.362	3.8	108.0	33.9	40.0	0.269	2.9	110.1	della Vedova et al. (2001)
MS1	AFT	44.134	9.638	0.000	0.136	25.0	31.3	0.367	3.8	108.1	33.8	40.0	0.276	2.9	110.3	della Vedova et al. (2001)
MS2	AFT	44.134	9.638	0.000	0.136	25.0	33.1	0.462	4.1	115.9	32.0	40.0	0.367	3.2	116.4	della Vedova et al. (2001)
MS4	AFT	44.134	9.638	0.000	0.136	25.1	32.8	0.442	4.1	115.2	32.3	40.0	0.347	3.2	115.6	della Vedova et al. (2001)
MS5	AFT	44.134	9.638	0.000	0.136	25.1	32.2	0.413	4.0	113.7	33.0	40.0	0.317	3.1	114.5	della Vedova et al. (2001)

https://doi.org/10.5194/se-2021-96
Preprint. Discussion started: 10 August 2021

PR 11	AFT	44.463	9.930	0.880	0.808	25.0	32.9	0.452	4.2	114.4	32.0	40.0	0.361	3.3	115.1	della Vedova et al. (2001)
PR 12	AFT	44.353	9.776	0.668	0.700	25.0	32.6	0.438	4.1	114.0	32.4	40.0	0.344	3.2	115.0	della Vedova et al. (2001)
PR 15	AFT	44.472	9.966	1.085	0.837	25.1	34.8	0.543	4.3	117.7	30.1	40.0	0.466	3.6	118.0	della Vedova et al. (2001)
PR 17	AFT	44.379	10.196	0.860	1.001	25.0	39.6	0.770	4.5	122.9	32.8	47.5	0.617	3.5	123.1	della Vedova et al. (2001)
PR 18	AFT	44.380	10.194	0.780	1.001	25.0	37.9	0.693	4.5	121.5	34.6	47.5	0.522	3.3	121.5	della Vedova et al. (2001)
PR 20	AFT	44.338	10.528	0.500	0.881	25.0	46.6	1.068	4.7	127.6	16.4	37.5	1.451	7.2	127.5	della Vedova et al. (2001)
PR 22	AFT	44.331	10.564	1.082	0.851	25.0	49.7	1.186	4.8	129.0	14.9	37.5	1.634	7.9	127.9	della Vedova et al. (2001)
PR 23.1	AFT	44.329	10.562	1.111	0.861	25.0	39.5	0.762	4.5	122.3	23.2	37.5	0.807	4.8	122.2	della Vedova et al. (2001)
PR 25.1	AFT	44.320	9.995	0.248	0.639	25.0	33.3	0.471	4.2	116.5	34.5	42.5	0.339	3.1	116.7	della Vedova et al. (2001)
PR 26	AFT	44.463	9.602	1.135	0.883	25.0	37.8	0.688	4.4	120.9	27.1	40.0	0.647	4.1	121.3	della Vedova et al. (2001)
PR 27	AFT	44.525	9.824	0.618	0.726	25.0	37.9	0.696	4.4	121.6	24.6	37.5	0.705	4.5	121.3	della Vedova et al. (2001)
PR 28.1	AFT	44.522	9.931	0.710	0.776	25.0	43.2	0.930	4.6	125.4	17.4	35.0	1.208	6.6	125.1	della Vedova et al. (2001)
PR 28.2	AFT	44.522	9.931	0.702	0.776	25.0	39.8	0.776	4.5	122.7	20.5	35.0	0.908	5.5	122.8	della Vedova et al. (2001)
PR 3	AFT	44.446	9.943	0.600	0.817	25.0	34.9	0.548	4.3	118.1	30.2	40.0	0.461	3.6	118.6	della Vedova et al. (2001)
PR 5	AFT	44.456	9.804	0.718	0.777	25.0	33.4	0.476	4.2	115.9	29.2	37.5	0.414	3.6	116.5	della Vedova et al. (2001)
PR 6.1	AFT	44.456	9.783	0.600	0.789	25.1	38.7	0.728	4.5	122.2	23.8	37.5	0.757	4.7	121.9	della Vedova et al. (2001)
PR 7	AFT	44.550	9.940	0.301	0.748	25.0	36.2	0.615	4.4	120.2	23.7	35.0	0.645	4.6	120.0	della Vedova et al. (2001)
RAM1	AFT	44.434	9.311	1.318	0.632	25.0	34.3	0.524	4.2	115.7	30.4	40.0	0.451	3.5	116.8	della Vedova et al. (2001)
RAM3	AFT	44.427	9.312	1.075	0.606	25.1	36.4	0.620	4.3	119.4	28.5	40.0	0.563	3.8	119.8	della Vedova et al. (2001)
RAM4	AFT	44.427	9.312	1.075	0.606	25.0	35	0.555	4.3	117.6	29.9	40.0	0.484	3.6	118.4	della Vedova et al. (2001)
RAM5	AFT	44.422	9.311	0.950	0.587	25.0	34.9	0.554	4.3	117.8	29.9	40.0	0.480	3.6	118.4	della Vedova et al. (2001)
RAM6	AFT	44.422	9.311	0.948	0.587	25.0	36	0.606	4.3	119.2	28.9	40.0	0.542	3.8	119.7	della Vedova et al. (2001)
ROM1	AFT	44.002	11.472	0.890	0.562	25.0	37.7	0.682	4.4	120.9	16.8	29.0	0.918	6.4	119.7	Pauselli et al. (2019)
ROM2	AFT	44.001	11.472	0.760	0.560	25.0	38.3	0.712	4.4	121.7	16.2	29.0	0.986	6.7	120.4	Pauselli et al. (2019)
ROM3	AFT	44.000	11.475	0.675	0.560	25.0	41.1	0.839	4.5	123.8	13.8	29.0	1.280	8.0	122.5	Pauselli et al. (2019)
ROM4	AFT	43.998	11.477	0.575	0.563	25.0	40.3	0.802	4.5	123.3	14.4	29.0	1.208	7.7	122.4	Pauselli et al. (2019)
ROM5	AFT	43.994	11.477	0.480	0.562	25.0	34.6	0.535	4.3	117.8	19.4	29.0	0.667	5.5	117.4	Pauselli et al. (2019)
S 1	AFT	44.178	10.160	0.546	0.662	25.1	34.7	0.539	4.3	118.0	32.9	42.5	0.421	3.3	118.5	della Vedova et al. (2001)
S 3	AFT	44.139	10.073	0.494	0.374	25.1	35.1	0.559	4.2	118.4	32.3	42.5	0.451	3.3	118.9	della Vedova et al. (2001)
S 4	AFT	44.128	10.059	0.636	0.330	25.0	38.3	0.714	4.4	121.6	28.9	42.5	0.640	3.8	121.8	della Vedova et al. (2001)
SC 2	AFT	44.081	10.083	0.204	0.342	25.1	34.6	0.534	4.2	118.1	30.5	40.0	0.448	3.5	118.4	della Vedova et al. (2001)
SILL1	AFT	44.368	10.064	1.861	0.860	25.0	35	0.560	4.3	116.2	33.9	44.5	0.453	3.2	118.0	della Vedova et al. (2001)
SILL10	AFT	44.334	10.050	0.730	0.754	25.1	34.3	0.516	4.3	117.1	35.3	44.5	0.381	3.0	118.0	della Vedova et al. (2001)
SILL2	AFT	44.361	10.074	1.790	0.863	25.1	34	0.503	4.1	111.6	35.4	45.0	0.394	3.0	114.4	della Vedova et al. (2001)
SILL3	AFT	44.357	10.073	1.600	0.853	25.0	37.1	0.659	4.4	120.0	32.3	45.0	0.551	3.4	121.0	della Vedova et al. (2001)
SILL4	AFT	44.455	10.076	1.530	0.951	25.0	38.1	0.704	4.5	121.2	26.8	40.0	0.671	4.2	121.4	della Vedova et al. (2001)
SILL5	AFT	44.354	10.071	1.420	0.843	25.0	36.3	0.620	4.4	119.2	33.2	45.0	0.503	3.3	120.2	della Vedova et al. (2001)
SILL6	AFT	44.353	10.057	1.260	0.815	25.0	35.9	0.602	4.4	118.9	33.1	44.5	0.484	3.3	119.5	della Vedova et al. (2001)
SILL7	AFT	44.338	10.058	1.130	0.781	25.0	36.7	0.639	4.4	120.0	32.4	44.5	0.524	3.4	120.4	della Vedova et al. (2001)
SILL9	AFT	44.334	10.050	0.780	0.755	25.0	37.1	0.658	4.4	120.5	32.2	44.5	0.534	3.4	121.0	della Vedova et al. (2001)
SM 3	AFT	44.164	10.129	0.250	0.558	25.0	31.9	0.398	4.1	113.1	35.9	42.5	0.274	2.9	114.0	della Vedova et al. (2001)
SU 1	AFT	44.170	10.188	0.773	0.724	25.0	35.1	0.566	4.3	118.6	32.3	42.5	0.454	3.4	119.1	della Vedova et al. (2001)
TCGA	AFT	43.993	11.476	0.360	0.560	25.0	36.8	0.643	4.4	120.6	17.2	29.0	0.877	6.3	119.7	Pauselli et al. (2019)
VALD1	AFT	43.594	11.603	0.497	0.484	25.0	37.6	0.681	4.4	121.3	16.7	29.0	0.937	6.5	120.1	Pauselli et al. (2019)
VALD10	AFT	43.653	11.640	1.400	0.836	25.0	35.6	0.582	4.3	118.1	18.3	28.5	0.740	5.8	116.9	Pauselli et al. (2019)
VALD11	AFT	43.663	11.641	1.450	0.644	25.0	38.1	0.701	4.4	120.8	15.9	28.0	0.962	6.8	119.3	Pauselli et al. (2019)
VALD12	AFT	43.696	11.673	0.960	0.717	25.0	35.6	0.582	4.3	118.5	17.7	28.0	0.769	6.1	117.5	Pauselli et al. (2019)
VALD2	AFT	43.612	11.645	0.500	0.550	25.0	33.8	0.495	4.2	116.6	21.2	30.0	0.573	4.9	116.1	Pauselli et al. (2019)
VALD3	AFT	43.614	11.656	0.580	0.559	25.0	34.7	0.541	4.3	117.8	20.4	30.0	0.646	5.2	117.5	Pauselli et al. (2019)
VALD4	AFT	43.620	11.648	0.740	0.567	25.0	37.4	0.673	4.4	120.9	17.4	29.5	0.888	6.2	119.9	Pauselli et al. (2019)
VALD5	AFT	43.621	11.656	0.850	0.572	25.0	40.1	0.796	4.5	123.1	15.7	30.0	1.109	7.0	121.8	Pauselli et al. (2019)
VALD6	AFT	43.620	11.659	0.880	0.571	25.0	35.4	0.575	4.3	118.3	19.8	30.0	0.692	5.4	117.6	Pauselli et al. (2019)
VALD7	AFT	43.604	11.651	1.100	0.536	25.0	36	0.606	4.3	119.0	20.2	31.0	0.709	5.3	118.0	Pauselli et al. (2019)
VALD8	AFT	43.626	11.684	1.200	0.585	25.0	33.9	0.503	4.2	115.2	21.7	30.5	0.562	4.7	114.2	Pauselli et al. (2019)
VALD9	AFT	43.646	11.652	1.200	0.619	25.0	34.1	0.512	4.2	115.7	20.1	29.0	0.608	5.1	114.4	Pauselli et al. (2019)
ZAT2	AFT	44.391	9.442	1.349	0.637	25.0	33.5	0.483	4.0	112.2	31.2	40.0	0.408	3.3	113.7	della Vedova et al. (2001)

Kinetic Parameters for FT apatite *(from Ketcham et al., 1999)*

E_a = 147 kJ mol^{-1} (activation energy)

Ω = 2.05 x 10^6 (measured directly from annealing experiments)

$t_{c,10}$ = 116°C (effective closure temperature for 10 Myr^{-1} cooling rates)

300

Table 10 Erosion rates and parameters for AFT detrital samples.

https://doi.org/10.5194/se-2021-96
Preprint. Discussion started: 10 August 2021

					Imposed G_0 = 25 (°C/km)					G_f calculated from heat flow measurements					
ID	Method	Latitude	Longitude	Sample Elevation (km)	Geothermal Gradient (°C/km)	Geothermal Gradient (°C/km)	Erosion Rate (km/My)	Closure Depth (km)	Closure Temperature (°C)	Inital Geothermal Gradient (°C/km)	Final Geothermal Gradient (°C/km)	Erosion Rate (km/My)	Closure Depth (km)	Closure Temperature (°C)	Heat Flow Measurement Source
Enza	AFT Detrital	44.620	10.413	0.163	25.0	38.0	0.699	4.3	121.5	12.5	25.0	1.189	8.5	120.1	della Vedova et al. (2001)
Nure	AFT Detrital	44.872	9.647	0.208	25.0	39.7	0.775	4.4	123.0	12.1	26.0	1.327	8.9	121.2	della Vedova et al. (2001)
Panaro	AFT Detrital	44.477	11.027	0.099	25.0	34.2	0.517	4.2	117.3	13.3	22.5	0.882	7.6	115.2	della Vedova et al. (2001)
Secchia	AFT Detrital	44.532	10.758	0.119	25.0	34.7	0.543	4.2	118.1	9.9	19.5	1.173	10.3	114.9	della Vedova et al. (2001)
Taro	AFT Detrital	44.713	10.120	0.117	25.0	38.2	0.710	4.3	121.7	14.7	27.5	1.067	7.3	120.7	della Vedova et al. (2001)
Trebbia	AFT Detrital	44.901	9.584	0.140	25.0	39.9	0.789	4.4	123.2	11.0	25.0	1.439	9.8	121.3	della Vedova et al. (2001)
Bisenzio	AFT Detrital	43.928	11.126	0.102	25.0	36.6	0.637	4.3	120.4	19.5	31.0	0.779	5.5	119.8	Pauselli et al. (2019)
Lima1	AFT Detrital	44.000	10.560	0.097	25.0	36.4	0.628	4.3	120.2	28.4	40.0	0.563	3.7	120.2	della Vedova et al. (2001)
Lima2	AFT Detrital	44.091	10.760	0.544	25.0	35.5	0.582	4.3	118.8	34.4	45.0	0.442	3.1	119.6	della Vedova et al. (2001)
Magra1	AFT Detrital	44.188	9.925	0.036	25.0	37.0	0.654	4.3	120.6	27.9	40.0	0.597	3.8	120.6	della Vedova et al. (2001)
Magra2	AFT Detrital	44.387	9.887	0.251	25.0	36.9	0.651	4.3	120.5	27.9	40.0	0.592	3.9	120.6	della Vedova et al. (2001)
Pescia	AFT Detrital	43.929	10.693	0.105	25.1	33.1	0.459	4.1	115.6	34.4	42.5	0.343	3.0	116.2	della Vedova et al. (2001)
Serchio	AFT Detrital	44.192	10.306	0.525	25.0	33.7	0.494	4.2	116.6	33.8	42.5	0.377	3.1	117.2	della Vedova et al. (2001)
Vara	AFT Detrital	44.198	9.851	0.032	25.0	35.5	0.585	4.2	119.3	29.4	40.0	0.509	3.6	119.5	della Vedova et al. (2001)

Kinetic Parameters for FT apatite *(from Ketcham et al., 1999)*

E_a = 147 kJ mol^{-1} (activation energy)

Ω = 2.05 x 10^6 (measured directly from annealing experiments)

$t_{c,10}$ = 116°C (effective closure temperature for 10 Myr^{-1} cooling rates)

Table 11 Erosion rates and parameters for ZHe samples.

						Imposed G_0 = 25 (°C/km)					G_f calculated from heat flow measurements					
ID	Method	Latitude	Longitude	Sample Elevation (km)	Mean Elevation (km)	Inital Geothermal Gradient (°C/km)	Final Geothermal Gradient (°C/km)	Erosion Rate (km/My)	Closure Depth (km)	Closure Temperature (°C)	Inital Geothermal Gradient (°C/km)	Final Geothermal Gradient (°C/km)	Erosion Rate (km/My)	Closure Depth (km)	Closure Temperature (°C)	Heat Flow Measurement Source
020620-3	ZHe	44.122	10.068	0.756	0.395	25	38.2	0.71	6.6	178.1	27	40	0.667	6.23	179.4	della Vedova et al. (2001)
020620-3 rep	ZHe	44.122	10.068	0.756	0.395	25	38.3	0.71	6.7	179.0	27	40	0.675	6.29	180.1	della Vedova et al. (2001)

Kinetic Parameters for (U-Th)/He zircon *(from Reiners et al., 2004)*

E_a = 169 kJ mol^{-1} (activation energy)

a_s = 60 μm (effective spherical radius for the diffusion domain)

Ω = 7.03 x 10^5 (frequency factor calculated as 55D_0a^{-2})

$t_{c,10}$ = 183°C (effective closure temperature for 10 Myr^{-1} cooling rates and specified a_s value)

https://doi.org/10.5194/se-2021-96
Preprint. Discussion started: 10 August 2021

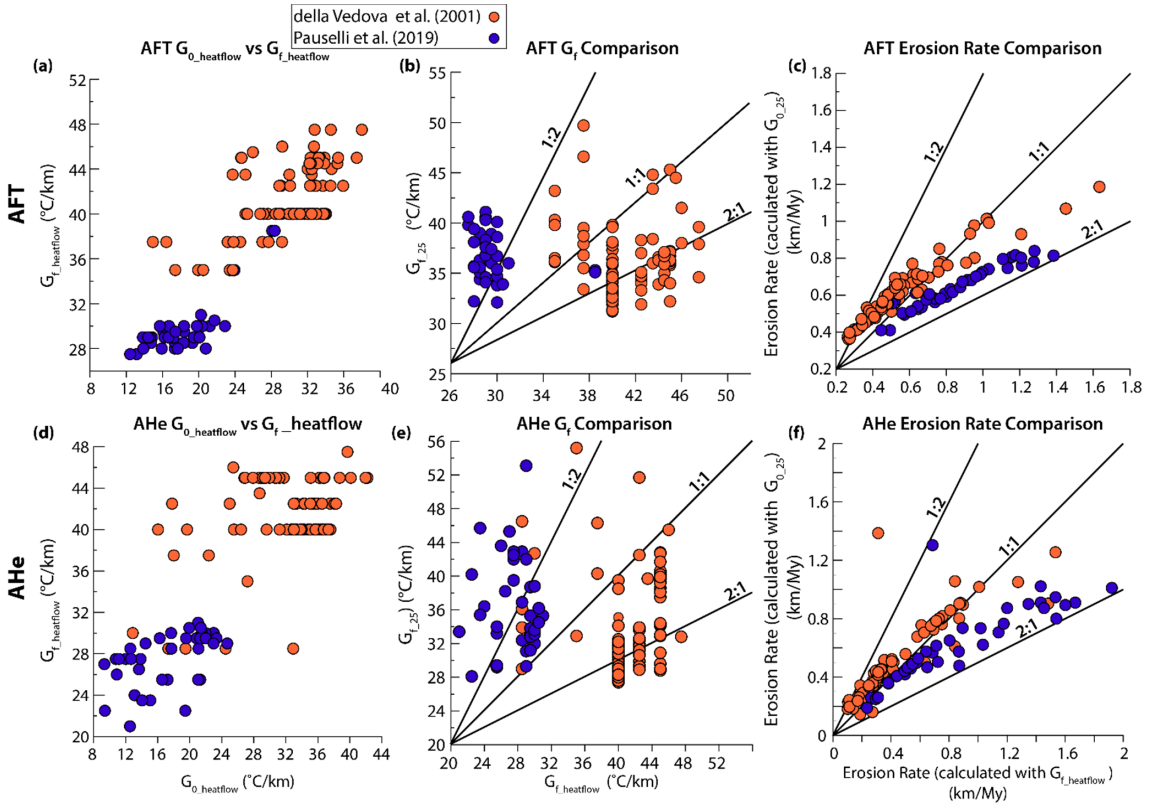

Figure 6 Comparison of initial geothermal gradients (G_0) and final geothermal gradients (G_f) for AFT samples (a–c) and AHe samples (d–f). (a) and (d) Comparison of $G_{0\_heatflow}$ and $G_{f\_heatflow}$. (b) and (e) Comparison of $G_{f\_heatflow}$ with G_{f_25}. (c) and (f) Comparison of erosion rates derived from $G_{f\_heatflow}$ measurements versus erosion rates derived from imposed G_{0_25}.

310

Here, we present the erosion rate results for the Adriatic and Ligurian sides of the orogen. Calculated with G_{0_25}, erosion rates inverted from AFT bedrock ages (Table 9; top row, Fig. 8) vary between 0.41 km/My and 1.19 km/My on the Adriatic side (Fig. 7d) and between 0.36 km/My and 0.84 km/My on the Ligurian side (Fig. 7c). The highest erosion rates on the Ligurian side are located in the Macigno Unit near the Alpi Apuane, whereas the highest rates on the Adriatic side are located near the

315 drainage divide (Cervarola Unit; top row, Fig. 8). AFT bedrock erosion rates across the divide are similar or slightly higher on the Adriatic side (Fig. 7c–d, top row, Fig. 8). AFT detrital erosion rates are similar to bedrock AFT rates, which also exhibit erosion rates that are higher on the Adriatic side (top row, Fig. 8). Erosion rates derived from AHe ages (Table 8) range between 0.14 and 1.39 km/My on the Adriatic side and between 0.14 and 0.74 km/My on the Ligurian side. AHe erosion rates on the Adriatic side are more variable relative to the Ligurian side, particularly in the southeast region of the field area (Fig. 7c–d).

https://doi.org/10.5194/se-2021-96
Preprint. Discussion started: 10 August 2021

Similar to the bedrock AFT erosion rates, the highest AHe erosion rates are found on the Adriatic side near the drainage divide and are lowest near the Ligurian coastline (top row, Fig. 8).

Calculated with $G_{f\_heatflow}$, the pattern of erosion across the drainage divide is similar to the pattern for erosion rates calculated with G_{0_25} (middle row, Fig. 8). On the Adriatic side, erosion rates inverted from AFT bedrock and detrital ages vary between 0.34 and 1.63 km/My and between 0.88 and 1.44 km/My, respectively. On the Ligurian side, AFT bedrock erosion rates vary between 0.26 and 1.28 km/My, and detrital AFT erosion rates vary between 0.34 and 0.78 km/My. Erosion rates derived from AHe ages range from 0.17 to 1.92 km/My on the Adriatic side and from 0.10 to 1.02 km/My on the Ligurian side. Detrital AFT erosion rates on the Adriatic side are higher relative to the Ligurian side, regardless of the method used for constraining the geothermal gradient. However, calculated from $G_{f\_heatflow}$, detrital AFT erosion rates on the Adriatic side are up to a factor of two higher than erosion rates calculated with G_{0_25} (Fig. 8).

https://doi.org/10.5194/se-2021-96
Preprint. Discussion started: 10 August 2021

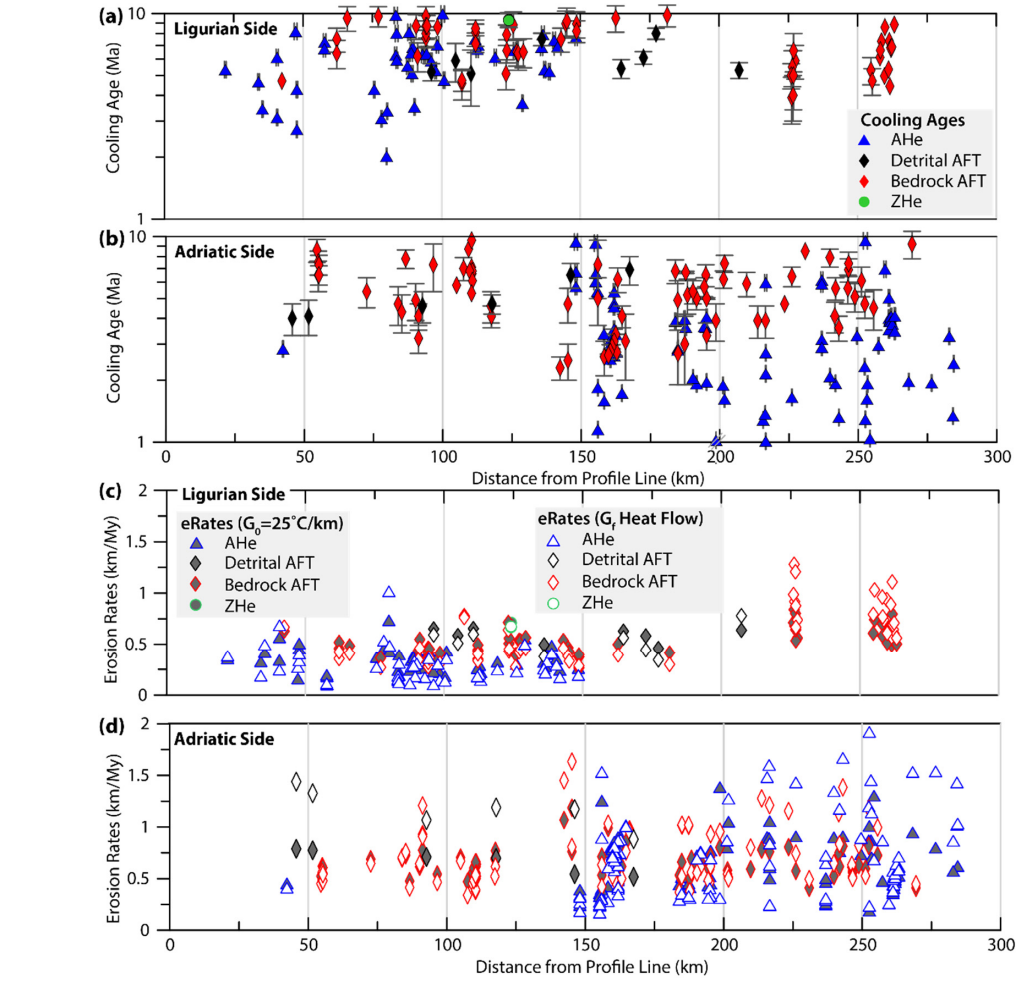

Figure 7 Cooling ages for all thermochronometers plotted along the Adriatic side (a) and the Ligurian side (b). Erosion rates for the (c) Adriatic side and (d) Ligurian side. Profile location for all plots is illustrated in Fig. 3a. In (b), individual AHe symbol dated to <1 Ma is illustrated with a double gray slash.

https://doi.org/10.5194/se-2021-96
Preprint. Discussion started: 10 August 2021

Solid Earth
Discussions
Open Access
EGU

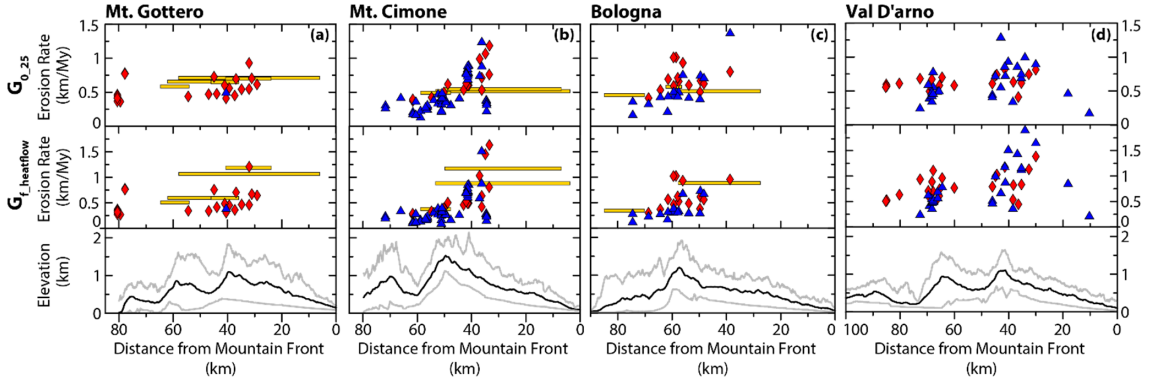

Figure 8 Erosion rates for AHe, bedrock AFT, and detrital AFT thermochronometers calculated from G_{0_25} (left column, a-d) or calculated with $G_{f\_heatflow}$ (right column, a-d). Length of the detrital AFT boxes reflects the distance from sample location to the catchment headwaters where the erosion rate is valid. Swath profile locations are shown in Fig. 3a. In the Bologna swath profile (right column), one AHe sample could not be resolved for an erosion rate with $G_{f\_heatflow}$.

3.3 Paired ages

Of the 30 paired samples analyzed here, erosion rates for two samples could not be resolved (Table 12), due to the similarity in ages between the AFT and AHe thermochronometers (sample C16) or due to an AHe age that is older than the AFT age (sample C22). Six paired samples are located on the Ligurian side of the orogen, and the remaining 22 samples are located on the Adriatic side of the orogen (Fig. 9).

Erosion rates from samples on the Adriatic side vary from ~0.3 to 5.2 km/My (Table 12). Twelve samples illustrate an increase in erosion through time (Fig. 9a), with the shift generally occurring between ~1 and 2 Ma. Ten samples from the Adriatic side illustrate a decrease in erosion rate through time (Fig. 9b), with the shift generally occurring between ~2 and 4 Ma. With the exception of three samples (AP53, AP57, and C29), decelerating sites are located in the headwaters of the Reno River (inset map, Fig. 9c), which drains the Cervarola and Macigno Units east of Mt. Cimone (Fig. 1). For the six paired samples from the Ligurian side, the range of erosion rates is similar and varies from ~0.3 to 5.1 km/My (Table 12). However, only one sample on the Ligurian side illustrates an increase in erosion rate, occurring at ~3 Ma (Fig. 9c). All other samples illustrate a decrease in erosion through time, with the shift occurring between ~6 and 2 Ma (Fig. 9d).

https://doi.org/10.5194/se-2021-96
Preprint. Discussion started: 10 August 2021

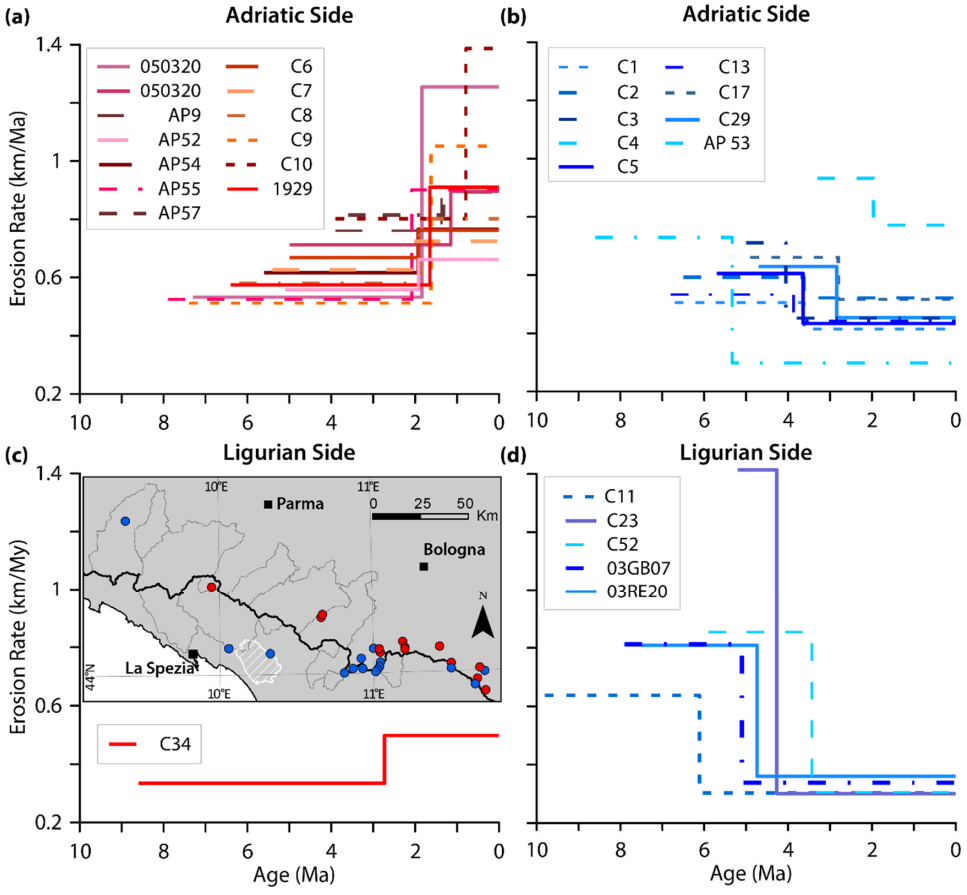

355

Figure 9 Erosion rates through time from paired AFT and AHe age samples on the Adriatic side for (a) increasing erosion rates and (b) decreasing erosion rates, and on the Ligurian side for (c) increasing erosion rates and for (d) decreasing erosion rates. Inset map in (c) shows the locations of paired thermochronometer age samples (circles). Red circles indicate locations where the erosion rate through time is increasing, and blue circles indicates locations where the erosion rate through time is decreasing.

360

Table 12 Erosion rates and parameters for paired AFT-AHe thermochronometer samples.

https://doi.org/10.5194/se-2021-96
Preprint. Discussion started: 10 August 2021

Solid Earth Discussions

	ID	Latitude	Longitude	Sample Elevation (km)	Method	Corrected Age (Ma)	Mean Elevation (km)	t_1 (Ma)	G_0 (°C/km)	G_f (°C/km)	Erosion Rate (km/My)	D_c (km)	T_c (°C)	Method	Mean Elevation (km)	t_1 (Ma)	G_0 (°C/km)	G_f (°C/km)	Erosion Rate (km/My)	D_c (km)	T_c (°C)
Ligurian Side	C11	44.00	10.81	0.95	AFT	3.19	0.64	3.39	33.78	35.15	0.46	1.47	117.40	AHe	0.67	6.61	39.85	41.07	0.25	1.53	61.96
	C23	44.02	10.93	0.88	AFT	0.43	0.69	5.23	6.34	36.79	5.09	2.19	138.26	AHe	0.72	4.77	39.05	40.72	0.35	1.48	64.01
	C34	44.42	9.95	0.51	AFT	5.37	0.82	6.77	30.14	32.02	0.27	1.47	113.63	AHe	0.85	3.23	34.54	36.57	0.42	1.15	64.11
	C52	44.01	11.50	0.36	AFT	1.97	0.59	6.07	11.42	20.78	1.59	3.13	123.26	AHe	0.66	3.93	23.41	25.08	0.52	1.78	62.35
	03GB07	44.12	10.06	0.68	AFT	2.30	0.36	4.40	25.35	31.29	0.77	1.76	122.35	AHe	0.36	5.60	34.35	35.84	0.34	1.73	62.86
	03RE20	44.10	10.33	1.06	AFT	2.26	0.76	4.76	24.27	31.01	0.82	1.84	122.76	AHe	0.81	5.24	33.98	35.72	0.37	1.74	63.04
Adriatic Side	1929	44.04	11.50	0.70	AFT	4.25	0.62	7.85	13.16	16.43	0.61	2.61	114.70	AHe	0.70	2.15	18.23	22.72	1.61	2.66	67.83
	050320-1a	44.26	10.66	1.11	AFT	5.65	0.98	8.35	25.82	27.17	0.16	0.89	108.66	AHe	1.02	1.65	28.22	35.41	1.70	1.96	72.78
	050320-1b	44.26	10.66	1.11	AFT	2.66	0.98	7.66	24.38	30.40	0.53	1.40	119.45	AHe	1.02	2.34	32.04	36.54	0.96	1.77	69.28
	AP52	43.91	11.72	0.57	AFT	2.68	0.80	7.58	9.81	16.26	1.21	3.26	119.27	AHe	0.84	2.42	18.23	21.66	1.27	2.44	66.08
	AP53	43.93	11.66	0.91	AFT	2.77	0.81	4.17	16.30	20.55	1.02	2.84	119.53	AHe	0.81	5.83	24.20	25.47	0.39	2.09	60.74
	AP 54	43.96	11.67	0.69	AFT	3.17	0.75	7.57	11.58	16.74	0.93	2.95	117.93	AHe	0.81	2.43	18.68	22.33	1.31	2.52	66.51
	AP 55	44.01	11.69	1.07	AFT	5.32	0.67	7.42	13.60	15.55	0.49	2.60	112.30	AHe	0.72	2.58	17.52	21.41	1.50	3.13	67.07
	AP 57	44.00	11.72	0.45	AFT	1.78	0.69	8.18	6.12	15.23	2.04	3.62	122.67	AHe	0.75	1.82	16.93	21.92	1.93	2.55	68.58
	AP9	44.12	11.43	0.40	AFT	2.03	0.67	8.13	7.33	15.42	1.66	3.38	121.43	AHe	0.67	1.87	17.12	22.00	1.84	2.52	68.13
	C1	44.11	11.00	0.50	AFT	2.58	0.79	5.88	25.88	32.66	0.67	1.72	121.30	AHe	0.76	4.12	35.25	36.82	0.32	1.16	62.44
	C10	44.14	11.19	0.61	AFT	2.61	0.68	8.71	12.44	17.76	0.75	1.97	117.30	AHe	0.77	1.29	18.98	28.02	2.92	2.31	73.22
	C13	44.02	10.86	0.70	AFT	2.43	0.73	5.63	32.26	39.36	0.58	1.41	122.14	AHe	0.75	4.37	41.97	43.76	0.30	1.17	63.40
	C16	44.06	10.91	0.63	AFT		0.81	NA	NA	NA	NA	NA	NA	AHe	0.91	NA	NA	NA	NA	NA	NA
	C17	44.07	10.92	0.63	AFT	1.60	0.82	6.70	23.57	37.11	1.08	1.72	126.83	AHe	0.92	3.30	39.53	41.55	0.37	1.03	64.26
	C2	44.00	11.01	0.83	AFT	2.38	0.55	5.88	28.32	35.73	0.66	1.57	122.59	AHe	0.66	4.12	38.26	40.39	0.42	1.52	65.06
	C22	44.04	10.93	0.85	AFT		0.75	NA	NA	NA	NA	NA	NA	AHe	0.82	NA	NA	NA	NA	NA	NA
	C29	44.73	9.39	0.32	AFT	1.36	0.80	6.66	13.37	27.72	1.75	2.38	127.55	AHe	0.77	3.34	30.05	31.87	0.43	1.22	63.09
	C3	44.01	11.03	0.78	AFT	0.45	0.58	5.45	6.08	36.98	5.15	2.32	138.07	AHe	0.71	4.55	39.29	40.93	0.34	1.38	63.95
	C4	44.03	11.04	0.68	AFT	0.84	0.62	7.54	11.77	33.02	2.29	1.93	132.26	AHe	0.75	2.46	34.89	38.48	0.74	1.45	68.27
	C5	44.05	11.04	0.61	AFT	1.56	0.68	5.86	21.50	34.80	1.23	1.92	126.81	AHe	0.80	4.14	37.54	39.10	0.32	1.17	63.09
	C6	44.10	11.04	0.65	AFT	2.58	0.74	7.58	23.04	29.78	0.61	1.57	120.27	AHe	0.78	2.42	31.58	35.10	0.80	1.54	68.05
	C7	44.11	11.04	0.63	AFT	2.85	0.74	7.45	24.02	30.05	0.54	1.53	119.02	AHe	0.75	2.55	31.88	35.26	0.74	1.51	67.35
	C8	44.12	11.21	0.70	AFT	3.81	0.68	7.61	22.86	26.72	0.42	1.60	116.20	AHe	0.76	2.39	28.51	32.28	0.94	1.77	68.29
	C9	44.11	11.20	1.00	AFT	5.28	0.67	7.88	22.23	24.01	0.26	1.39	111.75	AHe	0.74	2.12	25.51	30.82	1.40	2.27	70.19

3.4 Kinematic model

The orogenic wedge model shows how the spatial pattern of exhumation rates relates to the polarity of accretion and the pattern of horizontal and vertical motion. Figure 10 illustrates the predicted horizontal velocities, uplift rates, and material paths through the wedge for the spatially constant erosion rate setup (SCR) and the spatially variable erosion rate setup (VER). Horizontal velocities at the toes of the wedge are equal to the rate of slab rollback and decrease to a minimum at the drainage divide between the prowedge and retrowedge (Fig. 10a). Extension in the retrowedge results in higher horizontal erosion rates towards the Ligurian coast.

For the SCR setup, we ran the model with a single, orogen-wide erosion rate varying between 0.4 and 1.0 km/My, which are values consistent with average AHe-derived erosion rates for the Adriatic side of the orogen. Here, we illustrate the best-fit model results for an orogen-wide erosion rate of 0.8 km/My and a slab rollback rate (V_P) = 10 km/My. Horizontal velocities decrease to a minimum of 2.0 km/My at the drainage divide (Fig. 10a). Uplift rates on the prowedge vary from 0.89 to 1.1 km/My, and from 0.3 to 0.66 km/My on the retrowedge (Fig. 10b). Predicted reset cooling ages across the orogen for AHe samples (triangles) vary from 2.8 to 4.4 Ma, from 4.2 to 7.6 Ma for AFT (diamonds), and from 6.5 to 11.5 Ma for ZHe samples

https://doi.org/10.5194/se-2021-96
Preprint. Discussion started: 10 August 2021

(circles) (Fig. 11a, c). Maximum burial depth increases almost linearly across the orogenic wedge, ranging from 2.1 to 6.1 km on the prowedge and from 6.9 to 13.1 km on the retrowedge (Fig. 11b).

For the VER setup, we illustrate the best-fit model results for a prowedge erosion rate of 0.8 km/My and a retrowedge erosion rate of 0.4 km/My. Horizontal velocities decrease to a minimum of 2.0 km/My at the drainage divide (Fig. 10D). Uplift rates on the prowedge are the same as in the SCR (0.87–1.1 km/My), but uplift rates on the retrowedge are lower (-0.1–0.26 km/My) (Fig. 10e). Predicted reset cooling ages range from 3.8 to 5.8 Ma for AHe samples, from 6.2 to 8.3 Ma for AFT samples, and from 12.1 to 12.8 Ma for ZHe samples. For samples that reach the surface on the prowedge side of the range, predicted reset cooling ages decrease towards the primary divide. On the retrowedge, ages initially increase away from the divide, but young slightly at the model boundary (Fig. 11d). Maximum burial depth increases almost linearly along the prowedge (2.9–6.1 km) up to a kink at the drainage divide, which reflects the shift towards a shallower slope and smaller range of maximum burial depths along the retrowedge (6.9–9.4 km) (Fig. 11e).

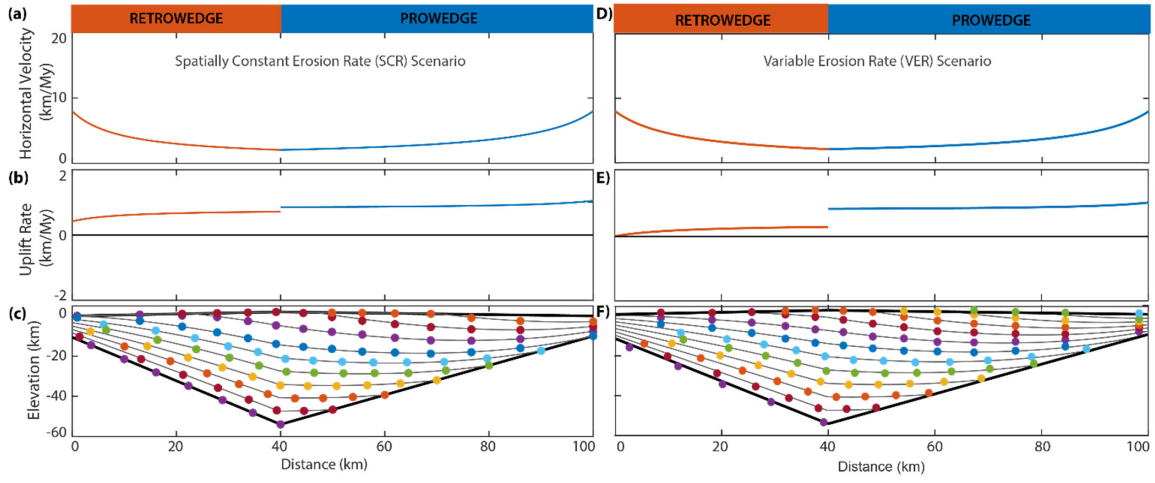

Figure 10 Kinematic model results. (a) Predicted material horizontal velocities across the orogenic wedge and (b) Predicted uplift rates across the wedge. (c) Material motion paths (lines within wedge) and particle positions and paths, equally spaced in time (solid, colored circles).

https://doi.org/10.5194/se-2021-96
Preprint. Discussion started: 10 August 2021

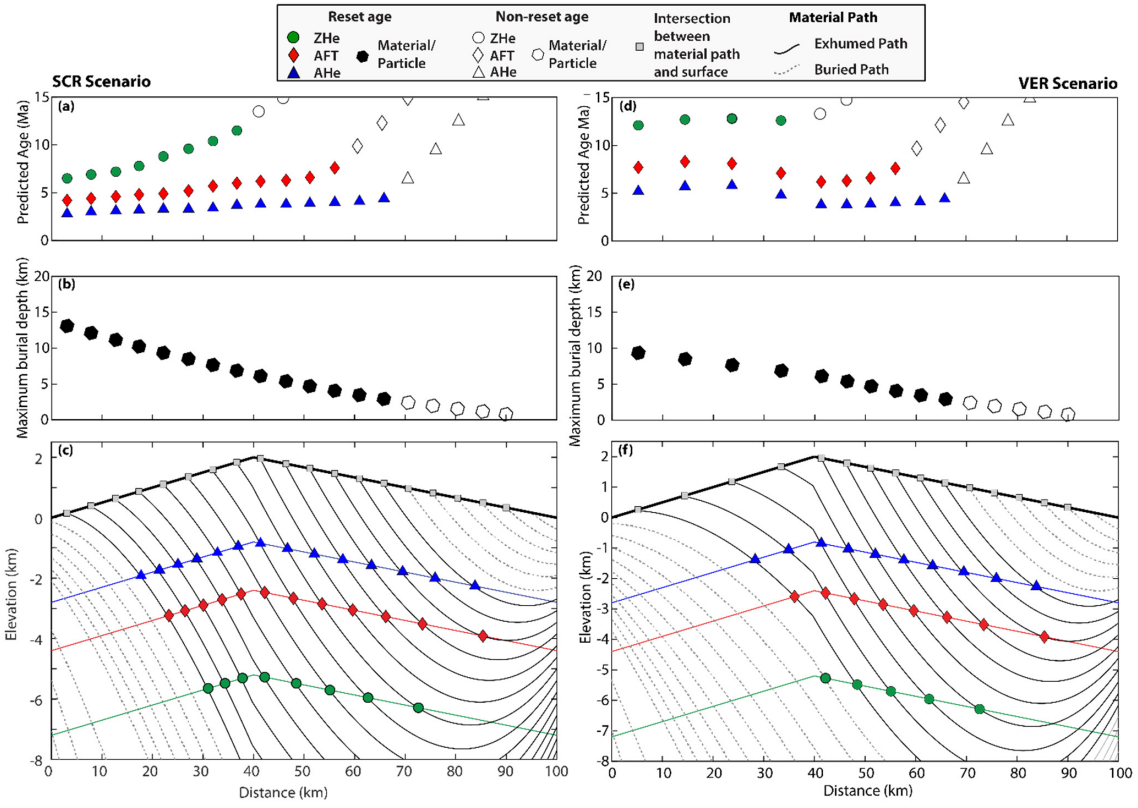

Figure 11 Closeup of kinematic model shown in Fig. 9. Left and right panels represent spatially constant erosion rate (SCR) and variable erosion rate (VER) model setups, respectively. (a) and (d) Predicted age of thermochronometers with distance along the wedge. (b) and (e) Predicted maximum burial depths for each particle path. (c) and (f) Material paths in upper 8 km of kinematic model. Colored lines illustrate closure depths for AHe, AFT, and ZHe thermochronometers.

4 Discussion

4.1 Detrital versus bedrock ages

Previous studies place the onset of exhumation between 8 and 14 Ma (Balestrieri et al., 1996; Ventura et al., 2001), so it is not clear whether the 12–13 Ma old population in the Vara and Magra samples represent partially or completely reset cooling ages. However, these ages are consistent with high-elevation samples west of the Vara catchment that record slow cooling prior to 8 Ma. The 8.2 Ma age peak is present in the Magra1 sample, which drains the extensional intermontane basin within the catchment, but is absent in the Magra2 sample, which drains only small tributaries upstream of the basin. Thus, the peak at 8.2 Ma in Magra1 likely reflects exhumation ages of the nearby Macigno Unit, which would have been eroded and redeposited

https://doi.org/10.5194/se-2021-96
Preprint. Discussion started: 10 August 2021

into the Pliocene basins (Balestrieri, 2000; Fellin et al., 2007). The pulse of exhumation in the Northern Apennines between 6 Ma and 4 Ma, when most of the Northern Apennines became sub-aerially exposed (Zattin et al., 2002; Balestrieri et al., 2003; Fellin et al., 2007), is consistent with the youngest peaks shown in the Vara, Magra, Lima, and Bisenzio Rivers.

The pattern of detrital AFT ages on the Ligurian and Adriatic sides (Malusà and Balestrieri, 2012) is consistent with the pattern of bedrock AFT ages, which illustrate younging exhumation ages towards the northeast, regardless of whether cooling ages are corrected or uncorrected for topography (Fig. 2). Overall, we find consistent results between the detrital AFT and bedrock AFT ages, reinforcing that the reset detrital ages illustrate a true exhumation signal, rather than an artefact of the technique. Fertility analysis of sediment from sampled Adriatic catchments also confirm that the detrital samples are representative of the eroded bedrock (Malusà et al., 2016), in the absence of hydraulic sorting effects. Finally, we note that using an initial exhumation age of 14 Ma would not change the pattern of exhumation, but would proportionally decrease all erosion rates in the Northern Apennines if the geothermal gradient increases in response to a longer period of erosion. As we incorporate only minimum reset ages from each sample, inclusion of the 13 Ma-year age population would have no effect on the erosion rate calculations.

4.2 Inferred erosion rate and relationship to the geothermal gradient

The geothermal gradient is the most important external parameter for converting cooling ages into erosion rates (Willett and Brandon, 2013). The two major studies of regional heat flow (della Vedova et al., 2001 and Pauselli et al., 2019) show large variations in heat flow across the region, but are also internally inconsistent by up to 50 mW/m^2 in the regions where they overlap. It is thus unclear how much of the spatial variability is real and how much is due to local effects or local errors in heat flow measurements, a large source of uncertainty for the geothermal gradients and ultimately, the erosion rates. To address this uncertainty, we took two approaches. First, we assumed that the initial geothermal gradient in the region was uniform and all variations in the modern geothermal gradient are due to advection in response to erosion. Second, we constrained the thermal model to be consistent with the modern heat flow measurements and inferred an initial geothermal gradient that was spatially variable.

The uncertainties in the modern heat flow measurements are evident in the erosion rate analysis, particularly when comparing the range of $G_{0\_heatflow}$ inferred from $G_{f\_heatflow}$ inputs that are calculated with heat flow measurements (Fig. 6a, d). However, it is unclear whether the large range of $G_{0\_heatflow}$ values represents how the geothermal gradient may have varied in either space or time at the onset of erosion. As the Northern Apennines evolved, sediments were accreted to the accretionary wedge shortly after being deposited in a subsiding foreland basin, whose modern equivalents are the Po Plain and the Adriatic Sea. There, modern heat flow values are generally low ($\leq$ 50 mW m^{-2}) (della Vedova et al. 2001), although with significant spatial variations (Pauselli et al., 2019), indicating that the present geothermal gradients in the foreland should be not higher than

https://doi.org/10.5194/se-2021-96
Preprint. Discussion started: 10 August 2021

about 30 ºC/km. Given the uncertainties on the modern heat flow measurements, the erosion analysis approach based on a common, G_{0_25} can be considered a viable alternative to the approach based on an input $G_{f\_heatflow}$.

The erosion rates resulting from these two analyses differ significantly: erosion rates from one analysis are a factor of two different from the alternate analysis (Fig. 6). However, the two sets of results projected along swath profiles from SW to NE show little difference in their spatial patterns across the main Apenninic divide (Fig. 8). The main differences are that the erosion rates derived from $G_{f\_heatflow}$ vary over a larger and higher range than those derived from G_{0_25}, and the maximum rates are higher from $G_{f\_heatflow}$. In particular, the youngest detrital age populations give much larger rates on the Adriatic side than on the Ligurian side with the analysis based on $G_{f\_heatflow}$. These observations suggest that the erosion rates derived from G_{0_25} may be more conservative estimates overall. However, the most important observation for the scope of this contribution remains that the large-scale spatial pattern of erosion rates along the swath profile does not change with the employed analysis method.

4.3 Erosion rate patterns

Bedrock cooling ages on the Ligurian side of the Northern Apennines generally vary between 4 and 10 Ma, with only a few ages younger than 4 Ma. On the Adriatic side, bedrock cooling ages younger than 4 Ma are a large component of the age distributions, especially among the AHe ages (Fig. 7b). Similarly, the youngest populations for detrital AFT samples on the Ligurian side are nearly all older than the youngest detrital AFT populations on the Adriatic side (Fig. 7a-b).

Erosion rates derived from both bedrock and detrital thermochronometric ages suggest a difference between the Ligurian and Adriatic sides that is valid at the regional scale, regardless of the method used for constraining the geothermal gradients. An exception to this general pattern may be the Alpi Apuane massif, which represents a structural culmination exposing a deep section. It is likely that this exhumation reflects structural control that is unique to the Northern Apennines. On the Ligurian side, erosion rates derived from bedrock AFT ages tend to be higher than erosion rates obtained from bedrock AHe ages (Fig. 7C) reflecting a regional decrease in erosion rate. This is particularly evident in the region east of the Alpi Apuane, at the main drainage divide north of Florence and in the Val d'Arno (Fig. 1 and 2). In contrast, on the Adriatic side, erosion rates derived from AHe ages tend to be higher than erosion rates obtained from AFT ages (Fig. 7D) and suggest an increase in erosion rate over the last 5 Ma.

Paired thermochronometers on the same sample (as for instance, AFT and AHe) or age-elevation transects (AETs) also indicate changes in erosion rate. The majority of the paired age samples (12) from the Adriatic side illustrate an increase in erosion rate through time (Fig. 9a), although 10 of these samples illustrate a decrease in erosion through time (Fig. 9b). Of these 10 samples, seven are from one region of the upper Reno River Valley (inset map, Fig. 9c). The headwaters of the Reno River Valley extend farther south than the adjacent basins of the Serchio River and Bisenzio River, which flow to the Ligurian Sea (Fig.

https://doi.org/10.5194/se-2021-96
Preprint. Discussion started: 10 August 2021

3a). Interestingly, the exhumation rates from the upper Reno River are similar to rates from the Serchio River, suggesting that the upper Reno River presents an erosion rate signal akin to Ligurian Rivers, rather than to Adriatic Rivers, and are thus resolving a consistent pattern of erosion rate in space, but not restricted to catchment boundaries. We also note that modern erosion rates from cosmogenic nuclide concentrations in the upper Reno tributaries are at least a factor of three lower than rates for the entire basin (Cyr et al., 2010), suggesting that this trend of lower erosion rates in this area has continued to the present.

Paired ages from the Ligurian side show the opposite trend. With the exception of one sample (C34) (Fig. 9c) located within the Magra2 catchment area (Fig. 3a), all other samples consistently illustrate a decrease in erosion rate through time (Fig. 9d). Thus, the results from the paired thermochronometer ages on the Adriatic and Ligurian sides of the orogen confirm the regional trends observed from the simple erosion rate analysis method.

The results from our paired ages analysis can also be discussed in the context of the AETs from Mt. Falterona, Mt. Cimone, and Val d'Arno (see Fig. 1 for locations). Between 4 and 2 Ma, these AETs have previously been interpreted to reflect an orogen-wide increase in exhumation and erosion rates, although there are notable differences between the results from the profiles on the Adriatic side (Mt Falterona and Mt. Cimone) and on the Ligurian side (Val d'Arno) (Thomson et al., 2010). The Mt. Falterona and Cimone AETs illustrate a two-fold increase in erosion rates between 4 and 5 Ma, from 0.29 ± 0.1 km/My to 0.58 ± 0.23 km/My and from 0.22 ± 0.09 km/My to 0.58 ± 0.16 km/My, respectively (Thomson et al., 2010). Excluding the samples from the upper Reno River Valley that illustrate a decrease in erosion rate through time, our paired ages analysis reflects erosion rates that increase from 0.68 ± 0.42 km/My to 1.31 ± 0.70 km/My, given 1s uncertainties. Our average erosion rates are higher than the average erosion rates calculated for the Mt. Falterona and Cimone AETs, although, given the high uncertainties in our values, they are within the range of the AETs.

The results from the Val d'Arno AET are less straightforward, due to the fact that some samples illustrate a decrease in erosion rate through time, while others illustrate an increase in erosion rate through time. When corrected for topographic and advection effects, this AET shows a negative slope that was previously interpreted to reflect post-cooling tilting of the footwall block of an extensional fault (Thomson et al., 2010). On the Ligurian side, cooling ages and erosion rates vary locally as a function of elevation and of fault activity, and extensional faults can control differences in the exhumation pattern. However, in light of our results from the simple analysis of erosion rates and the paired ages, this negative slope could also be interpreted as a decrease in erosion rates, and thus would reflect a regional signal, rather than local tectonics. We infer that such regional scale-differences must be controlled by first-order features of the Northern Apennines. In order to address the question of what could control such differences, we compare two different kinematic models for the Northern Apennines orogenic wedge.

https://doi.org/10.5194/se-2021-96
Preprint. Discussion started: 10 August 2021


Solid Earth Discussions

4.4 Kinematic model

The orogenic wedge kinematic models illustrate differences in cooling ages, maximum burial temperatures, and material paths across the Northern Apennines, assuming simple continuum accretion and mass balance (Fig. 11). Using a spatially constant erosion rate across the orogenic wedge (SCR) predicts that reset ages decrease from northeast to southwest and are youngest on the retrowedge model boundary. In contrast, the variable erosion rate setup (VER) predicts minimum reset ages near the drainage divide and maximum reset ages on the retrowedge, close to the model boundary. The VER model is consistent with observed cooling ages, which are youngest near the drainage divide in the core of the Northern Apennines (Fig. 2).

Vitrinite reflectance (VR) data provide an additional estimate for maximum paleotemperature and burial depth and thus, an additional calibration of the kinematic model. In the Northern Apennines, Ro values reach 5.1% at the Ligurian coastline along the Mt. Gottero swath profile (Fig. 2a). With the exception of this profile, maximum VR values are generally within the range of 1.5–2.5 % for the Mt. Cimone, Bologna, and Val d'Arno profiles (Fig. 2b-d). Maximum paleotemperatures from VR are estimated at 200-250°C in the core of the range and along the Ligurian coastline in the northwest (Fellin et al., 2007), whereas paleotemperatures are 150–190°C in the Cervarola Unit (VR = 1.0–1.7%), and are 100-110°C in the Ligurian Unit (VR = 0.5–0.6%) (Ventura et al., 2001; Botti et al., 2004). Maximum paleotemperatures should correspond to maximum burial depths; thus, we expect to find the maximum burial depths along the Ligurian coastline and near the drainage divide in the Cervarola Unit. Both the SCR and VER models predict maximum burial depths near the Ligurian coastline, consistent with the trends observed in the Mt. Gottero and Val d'Arno profile. Near the drainage divide on the prowedge, predicted maximum burial depths are 6.1 km for both models.

We can estimate maximum burial depths at the drainage divide, given the generalized relationship between Ro and burial depth (Suggate, 1998), VR values, and a modern geothermal gradient. To estimate the modern geothermal gradient at the drainage divide, we use $G_{f\_heatflow}$ rates from the simple erosion analysis for AHe samples in the Cervarola Unit (Tables 1 and 7). Given these parameters. we estimate maximum burial depths in the range of 4.0–5.5 km near the drainage divide; the upper bound of this range are similar to the predicted maximum burial depths (6.1 km) for both the SCR and VER models. Collectively, our erosion rate analysis and kinematic model illustrate that the east to west particle trajectories, combined with lower erosion rates on the retrowedge, are consistent with the spatial pattern of cooling ages and maximum paleotemperatures estimated from both vitrinite reflectance and thermochronometric data.

The particle paths in the VER kinematic model, combined with the lower erosion rates in the retrowedge, suggest an explanation for the apparent decrease in erosion rates with time on the Ligurian side of the Apennines. As rocks are advected from prowedge to retrowedge, the vertical component of their motion decreases (Fig. 10f). Particle paths where the AFT age

https://doi.org/10.5194/se-2021-96
Preprint. Discussion started: 10 August 2021

is set in the prowedge, but where the AHe is set in the retrowedge, will record this change as a temporal deceleration of cooling rate. However, rather than representing a change in surface erosion rate, the change in cooling rate reflects the motion of the rock from the fast erosion rate prowedge into the low erosion rate retrowedge. The fact that the decelerating sites are all found to the southwest, regardless of drainage basin (inset, Fig. 8c) supports the idea that this is a tectonically controlled spatial pattern.

The acceleration of exhumation observed in the prowedge is not explained by the kinematic model. Although the apparent increase in exhumation rate might be explained by spatial changes in tectonic uplift and an associated increase in erosion rate, there is no strong evidence for this in the spatial pattern of ages or in the geomorphology, which should show higher uplift rates in the range interior. In contrast, the highest uplift rates are more often observed at the mountain front (Picotti and Pazzaglia, 2008). It is more likely that this is a true temporal increase in erosion rate, which could be associated with an increase in accretionary flux as the mountain front advanced into the Alpine sediments of the Adriatic foreland. The foreland basin fill thickened as Miocene alpine sediments filled the foredeep and again in the Quaternary as glacial sediments filled the Po plain and parts of the Adriatic Sea. The increase in accretionary flux would lead to an increase in wedge size and in erosion rate, processes that our kinematic model does not include. The increase in erosion rate could also be associated with a direct, externally-driven increase in surface erosion rate associated with Quaternary climate change. Although the Apennines were not significantly affected by alpine glaciation, the cooling and strong cyclicity of the Quaternary climate may have led to an increase in erosion rate through the efficiency of periglacial processes and hillslope processes such as landsliding (Amorosi et al., 1996; Borgatti and Soldati, 2010; Simoni et al., 2013; Wegmann and Pazzaglia, 2009).

5 Conclusion

We present evidence from multiple thermochronometers that the spatial and temporal pattern of erosion rates in the Northern Apennines orogen differs at the regional scale. Time-averaged erosion rates from individual thermochronometers predict faster erosion rates derived from AHe ages on the Adriatic side relative to the Ligurian side. These results are consistent with erosion rates derived from paired AFT-AHe thermochronometer samples, which illustrate an increase in erosion rates through time on the Adriatic side, but a decrease in erosion rates through time on the Ligurian side. The pattern of erosion rates across the orogen is also consistent with a kinematic model for an asymmetric orogen that includes both frontal accretion and underplating modes of crustal accretion, a slab rollback rate of 10 km/My, and prowedge erosion rates that are a factor of two higher than retrowedge erosion rates. This model suggests that that observed decelerations on the retrowedge are the result of the spatial advection of rock to the SW, although the observed acceleration of erosion rates on the prowedge requires external forcing, either through an increase in accretionary flux or through more erosive conditions linked to climate change.

Code/Data Availability

https://doi.org/10.5194/se-2021-96
Preprint. Discussion started: 10 August 2021

All data used in this study are included in the text. Related codes for the erosion rate analysis and kinematic model are available upon request to the corresponding author.

Author Contribution

EDE, MGF and SDW collected the detrital AFT samples in Northern Apennine catchments. EDE and MGF processed and analyzed the detrital AFT samples. SDW wrote the kinematic model. EDE, MGF, and SDW all contributed to the interpretation of the data. EDE wrote the manuscript and created the figures, with input from MGF and SDW.

Competing Interests

The authors declare that they have no conflict of interest.

References

Abbate, E., Balestrieri, M. L., Bigazzi, G., Norelli, P. and Quercioli, C.: Fission track datings and recent rapid denudation in Northern Apennines, Mem. Soc. geol. it, 48, 579–585, 1994.

Abbate, E., Balestrieri, M. L., Bigazzi, G., Ventura, B., Zattin, M. and Zuffa, G. G.: An extensive apatite fission-track study throughout the Northern Apennines Nappe belt, Radiat. Meas., 31(1–6), 673–676, doi:Doi 10.1016/S1350-4487(99)00168-7, 1999.

Amorosi, A., Farina, M., Severi, P., Preti, D., Caporale, L. and Di Dio, G.: Genetically related alluvial deposits across active fault zones: An example of alluvial fan-terrace correlation from the upper Quaternary of the southern Po Basin, Italy, Sediment. Geol., 102(3–4), 275–295, doi:10.1016/0037-0738(95)00074-7, 1996.

Balestrieri, M. L.: Exhumation ages and block faulting on the eastern flank of the Serchio graben (northern Apennines), in 9th International Conference on Fission Track Dating and Thermochronology, Univ. of Melbourne Fission Track Res. Group, Lorne, Victoria, Australia., 2000.

Balestrieri, M. L., Abbate, E. and Bigazzi, G.: Insights on the thermal evolution of the Ligurian Apennines (Italy) through fission-track analysis, J. Geol. Soc. London., 153(3), 419–425, doi:10.1144/gsjgs.153.3.0419, 1996.

Balestrieri, M. L., Bernet, M., Brandon, M. T., Picotti, V., Reiners, P. W. and Zattin, M.: Pliocene and Pleistocene exhumation and uplift of two key areas of the Northern Apennines, Quat. Int., 101, 67–73, 2003.

Balestrieri, M. L., Benvenuti, M. and Catanzariti, R.: Unravelling basin shoulder dynamics through detrital apatite fission-track signature: the case of the Quaternary Mugello Basin, Italy, Geol. Mag., 155(7), 1413–1426, doi:10.1017/s0016756817000073, 2018.

Bertoldi, R.: Una sequenza palinologica di età rusciniana nei sedimenti lacustri basali del bacino di Aulla-Olivola (Val di Magra), Riv. Ital. di Paleontol. e Stratigr., 94(1), 105–138, 1988.

Borgatti, L. and Soldati, M.: Landslides as a geomorphological proxy for climate change: A record from the Dolomites

https://doi.org/10.5194/se-2021-96
Preprint. Discussion started: 10 August 2021

(northern Italy), Geomorphology, 120(1), 56–64, doi:https://doi.org/10.1016/j.geomorph.2009.09.015, 2010.

Botti, F., Aldega, L. and Corrado, S.: Sedimentary and tectonic burial evolution of the Northern Apennines in the Modena-Bologna area: constraints from combined stratigraphic, structural, organic matter and clay mineral data of Neogene thrust-top basins, Geodin. Acta, 17(3), 185–203, doi:10.3166/ga.17.185-203, 2004.

Brandon, M. T.: Decomposition of mixed grain age distributions using Binomfit, On track, 24(8), 13–18, 2002.

Carlini, M., Artoni, A., Aldega, L., Balestrieri, M. L., Corrado, S., Vescovi, P., Bernini, M. and Torelli, L.: Exhumation and reshaping of far-travelled/allochthonous tectonic units in mountain belts. New insights for the relationships between shortening and coeval extension in the western Northern Apennines (Italy), Tectonophysics, 608, 267–287, doi:10.1016/j.tecto.2013.09.029, 2013.

Cibin, U., Spadafora, E., Zuffa, G. G. and Castellarin, A.: Continental collision history from arenites of episutural basins in the Northern Apennines, Italy, Bull. Geol. Soc. Am., 113(1), 4–19, doi:10.1130/0016-7606(2001)113<0004:CCHFAO>2.0.CO;2, 2001.

Cita Sironi, M. B., Abbate, E., Balini, M., Conti, M. A., Germani, D., Groppelli, G., Manetti, P. and Petti, M. N.: Catalogo delle formazioni. Unità tradizionali, Cart. Geol. d'Italia, 1(50.000), 2006.

Cyr, A. J., Granger, D. E., Olivetti, V. and Molin, P.: Quantifying rock uplift rates using channel steepness and cosmogenic nuclide-determined erosion rates: Examples from northern and southern Italy, Lithosphere, 2(3), 188–198, doi:10.1130/L96.1, 2010.

Delfrati, L., Falorni, P., Gropelli, G. and Petti, F. M.: Catalogo delle formazioni-Unità tradizionali, Quaderni serie III, Vol 7, fasciolo III, Cart. Geol. d'Italia, scale, 1(50), 0, 2002.

Dodson, M. H.: Theory of cooling ages, in Lectures in isotope geology, pp. 194–202, Springer., 1979.

Faccenna, C., Becker, T. W., Miller, M. S., Serpelloni, E. and Willett, S. D.: Isostasy, dynamic topography, and the elevation of the Apennines of Italy, Earth Planet. Sci. Lett., 407, 163–174, doi:10.1016/j.epsl.2014.09.027, 2014.

Fellin, M. G., Reiners, P. W., Brandon, M. T., Wüthrich, E., Balestrieri, M. L. and Molli, G.: Thermochronologic evidence for the exhumational history of the Alpi Apuane metamorphic core complex, northern Apennines, Italy, Tectonics, 26(6), 1–22, doi:10.1029/2006TC002085, 2007.

Galbraith, R. F.: On statistical models for fission track counts, J. Int. Assoc. Math. Geol., 13(6), 471–478, 1981.

Hurford, A. J.: Standardization of fission track dating calibration: Recommendation by the Fission Track Working Group of the IUGS Subcommission on Geochronology, Chem. Geol. Isot. Geosci. Sect., 80(2), 171–178, 1990.

Hurford, A. J. and Green, P. F.: The zeta age calibration of fission-track dating, Chem. Geol., 41, 285–317, 1983.

Malinverno, A. and Ryan, W. B. F.: Extension in the Tyrrhenian Sea and shortening in the Apennines as result of arc migration driven by sinking of the lithosphere, Tectonics, 5(2), 227–245, 1986.

Malusà, M. G. and Balestrieri, M. L.: Burial and exhumation across the Alps-Apennines junction zone constrained by fission-track analysis on modern river sands, Terra Nov., 24(3), 221–226, doi:10.1111/j.1365-3121.2011.01057.x, 2012.

Malusà, M. G., Resentini, A. and Garzanti, E.: Hydraulic sorting and mineral fertility bias in detrital geochronology, Gondwana

https://doi.org/10.5194/se-2021-96
Preprint. Discussion started: 10 August 2021

Res., 31, 1–19, doi:10.1016/j.gr.2015.09.002, 2016.

Merla, G.: Geologia dell'Appennino settentrionale, Arti Grafiche Pacini Mariotti., 1952.

Ori, G. G. and Friend, P. F.: Sedimentary basins formed and carried piggyback on active thrust sheets., Geology, 12(8), 475–478, doi:10.1130/0091-7613(1984)12<475:SBFACP>2.0.CO;2, 1984.

Pauselli, C., Gola, G., Mancinelli, P., Trumpy, E., Saccone, M., Manzella, A. and Ranalli, G.: A new surface heat flow map of the Northern Apennines between latitudes 42.5 and 44.5 N, Geothermics, 81(March), 39–52, doi:10.1016/j.geothermics.2019.04.002, 2019.

Pialli, G., Plesi, G., Damiani, A. V, Brozzetti, F., Boscherini, A., Bucefalo Palliani, R., Cardinali, M., Checcucci, R., Daniele, G. and Galli, M.: Note illustrative del Foglio 289 «Città di Castello», Cart. Geol. d'Italia, scale, 1(50.000), 2000.

Picotti, V. and Pazzaglia, F. J.: A new active tectonic model for the construction of the Northern Apennines mountain front near Bologna (Italy), J. Geophys. Res. Solid Earth, 113(8), 1–24, doi:10.1029/2007JB005307, 2008.

Pini, G. A.: Tectonosomes and Olistostromes in the Argile Scagliose of the Northern Apennines, Geol. Soc. Am. Spec. Pap., 335, 70, doi:10.1130/0-8137-2335-3.1, 1999.

Reiners, P. W. and Brandon, M. T.: Using Thermochronology To Understand Orogenic Erosion, Annu. Rev. Earth Planet. Sci., 34(1), 419–466, doi:10.1146/annurev.earth.34.031405.125202, 2006.

Reutter, K. J., Teichmüller, M., Teichmüller, R. and Zanzucchi, G.: The coalification pattern in the Northern Apennines and its palaeogeothermic and tectonic significance, Geol. Rundschau, 72(3), 861–893, doi:10.1007/BF01848346, 1983.

Ricci Lucchi, F.: The Oligocene to Recent foreland basins of the northern Appennines, edited by A. Allen and P. Homewood, Forel. Basins, 105–139, doi:doi:10.1002/9781444303810.ch6, 1986.

Rosenbaum, G. and Piana Agostinetti, N.: Crustal and upper mantle responses to lithospheric segmentation in the northern Apennines, Tectonics, 34(4), 648–661, doi:10.1002/2013TC003498, 2015.

Simoni, A., Ponza, A., Picotti, V., Berti, M. and Dinelli, E.: Earthflow sediment production and Holocene sediment record in a large Apennine catchment, Geomorphology, 188, 42–53, doi:10.1016/j.geomorph.2012.12.006, 2013.

Spada, M., Bianchi, I., Kissling, E., Agostinetti, N. P. and Wiemer, S.: Combining controlled-source seismology and receiver function information to derive 3-D moho topography for italy, Geophys. J. Int., 194(2), 1050–1068, doi:10.1093/gji/ggt148, 2013.

Suggate, R. P.: Relations between depth of burial, vitrinite reflectance and geothermal gradient, J. Pet. Geol., 22(2), 5–32, doi:10.1111/j.1747-5457.1999.tb00471.x, 1998.

Thomson, S. N., Brandon, M. T., Reiners, P. W., Zattin, M., Isaacson, P. J. and Balestrieri, M. L.: Thermochronologic evidence for orogen-parallel variability in wedge kinematics during extending convergent orogenesis of the northern Apennines, Italy, Bull. Geol. Soc. Am., 122(7–8), 1160–1179, doi:10.1130/B26573.1, 2010.

Vai, F. and Martini, I. P.: Anatomy of an orogen: the Apennines and adjacent Mediterranean basins, Springer., 2001.

della Vedova, B., Bellani, S., Pellis, G. and Squarci, P.: Heat Flow Distribution, , 65–76, 2001.

Ventura, B., Pini, G. A. and Zuffa, G. G.: Thermal history and exhumation of the Northern Apennines (Italy): evidence from

https://doi.org/10.5194/se-2021-96
Preprint. Discussion started: 10 August 2021

combined apatitefissio-track and vitrinite reflectance data from foreland basin sediments., Basin Res., 435–448, 2001.

Wegmann, K. W. and Pazzaglia, F. J.: Late Quaternary fluvial terraces of the Romagna and Marche Apennines, Italy: Climatic, lithologic, and tectonic controls on terrace genesis in an active orogen, Quat. Sci. Rev., 28(1–2), 137–165, doi:10.1016/j.quascirev.2008.10.006, 2009.

Willett, S. D. and Brandon, M. T.: Some analytical methods for converting thermochronometric age to erosion rate, Geochemistry, Geophys. Geosystems, 14(1), 209–222, doi:10.1029/2012GC004279, 2013.

Willett, S. D., Slingerland, R. and Hovius, N.: Uplift, shortenning, and steady state topography in active mountain belts, Am. J. Sci., 301, 455–485, 2001.

Willett, S. D., Herman, F., Fox, M., Stalder, N., Ehlers, T. A., Jiao, R. and Yang, R.: Bias and error in modelling thermochronometric data: Resolving a potential increase in Plio-Pleistocene erosion rate, Earth Surf. Dyn. Discuss., 1–78, 2020.

Wilson, L. F., Pazzaglia, F. J. and Anastasio, D. J.: A Fluvial record of active fault-propagation folding, salsomaggiore anticline, northern Apennines, Italy, J. Geophys. Res. Solid Earth, 114(8), 1–23, doi:10.1029/2008JB005984, 2009.

Zattin, M., Picotti, V. and Zuffa, G. G.: Fission-track reconstruction of the front of the Northern Apennine thrust wedge and overlying Ligurian unit, Am. J. Sci., 302(4), 346–379, doi:10.2475/ajs.302.4.346, 2002.